Localized-Based Control Algorithm For Passenger Ride Comfort

by

Suk Jin Kim

A thesis
presented to the University of Waterloo
in fulfillment of the
thesis requirement for the degree of
Master of Applied Science
in
Mechanical Engineering

Waterloo, Ontario, Canada, 2014

AUTHOR'S DECLARATION

I hereby declare that I am the sole author of this thesis. This is a true copy of the thesis, including any required final revisions, as accepted by my examiners.

I understand that my thesis may be made electronically available to the public.

Abstract

In this thesis, a new localized-based suspension control strategy is developed, simulated and validated with experimental results. Basic concepts of mathematical vehicle models, suspension systems, and conventional control algorithms, namely skyhook, groundhook, and hybrid controllers, used for ride comfort and road holding are also studied and implemented for comparison.

The conventional control algorithms are for the vertical motion of a sprung mass, or an unsprung mass at each corner of a vehicle. The proposed localized-based control algorithm is a controller that can change its target location in a vehicle to where it is needed most. Simulation results show that the localized-based controller provides better ride comfort on targeted locations than the conventional control algorithms.

Experimental results using a Cadillac STS test vehicle are used to compare the localized-based control algorithm with the conventional algorithms in vehicle comfort and holding. The results show that the new controller improves ride comfort more than other controllers. The prospect of easily adapting the new control algorithm to various vehicles is promising.

Acknowledgements

First of all, I would like to express my gratitude to my supervisor, Dr. Amir Khajepour. He supported me with confidence and encouraged me to finish this thesis. Also, whenever I had some problems with my project, his advice helped me understand the core of the problem and solve them.

I also want to specially thank people in my office. Alireza Kasaiezadeh gave me some valuable advice to help my project. Kevin Cochran and Jeff Graansma helped me set up a vehicle for experiments and finish this project. Michael Karl Binder was working with me from the beginning to the end of the project and the project would not have been complete without him. I also thank Milad Jalali, Huang Yanjun, Milad Khazraee, Ehsan Asadi, Hasan Toplar, Yangtao Li, and Roberto Ribeiro for making my school life sociable and enjoyable during my masters.

Furthermore, I also thank Sriram Moorthy, who was my roommate for my entire two years. My life in Waterloo would have never been easy without him.

Finally, I want to specially thank my parents and my two sisters. They always took care of my health and academic progress although they lived in another city.

Table of Contents

List of Figures

List of Tables

Chapter 1
Literature Review and Background

Many mechanical components and control algorithms have been invented in order to provide better comfort and safety to passengers. Among these devices, a suspension system is one of the most effective elements in helping passengers feel more comfortable and safer [1][2]. In any suspension, the response of the sprung mass is mostly related to the passenger comfort while the response of the un-sprung mass is related to the vehicle road holding and dynamics.

Ironically, ride comfort and road holding always conflict with each other. A suspension system cannot provide an optimum response for both ride comfort and road holding simultaneously. Furthermore, as road conditions vary, the optimum solution changes calling for adaptive or active suspensions.

In this thesis, ride comfort and road holding for passengers are discussed as well as a new control algorithm for better ride comfort. In Chapter 1, literature review and background on vehicle models, suspension systems, and widely-used suspension control algorithms such as skyhook, groundhook, and hybrid are discussed. In Chapter 2, modelling of a vehicle with a suspension system along with road inputs including a bump and random road irregularities for simulation analysis are explained. Simulation results using the conventional suspension control algorithms are also presented. In Chapter 3, a new control algorithm (localized-based) is introduced and simulation results are presented. In Chapter 4, the new control algorithm is validated using a Cadillac STS test vehicle. In Chapter 5, conclusions and future work are discussed.

1.1 Vehicle Modelling and Formulation

This chapter introduces three different vehicle modelling and formulation methods: quarter, half, and full. In this section, the whole configuration of a vehicle including a rigid body (sprung mass), a wheel (unsprung mass), and a suspension system between the sprung mass and unsprung mass is modeled mathematically.

Next is a discussion of three types of suspension systems: passive, semi-active, and active. This is followed by an introduction to the many available methods to reduce vehicle vibration using a suspension system.

Lastly, conventional suspension control algorithms will be introduced. In this section, traditional and the most widely-used skyhook, groundhook, and hybrid (including both the skyhook and groundhook control algorithms) will be introduced. The skyhook control algorithm will be compared to the new control algorithm later.

A mathematical model is required to conduct simulations. In the following, some vehicle models used in this thesis are discussed.

1.1.1 Quarter Car Model

This subsection explains the quarter car model for modeling and formulating a vehicle. It is the most simplified model among the vehicle models discussed in this chapter.

As shown in Figure 1, the quarter car model has only one quarter of the rigid body of a vehicle (sprung mass), a wheel (unsprung mass), and a suspension system between the sprung mass and the unsprung mass. The suspension system has a spring and a damping element. The tire of the unsprung mass is modeled as a spring as shown in the figure.

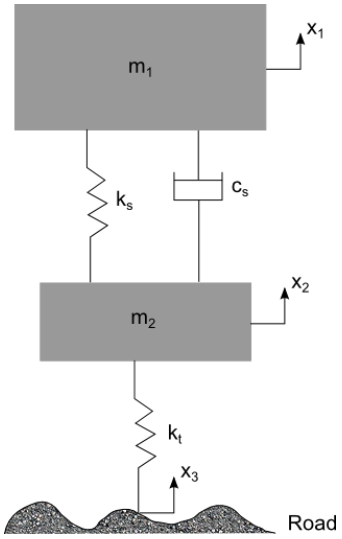

Figure 1: Quarter Car Model

The quarter car model is a two degree of freedom system. It has a spring, k_s, and a damper, c_s, which are connected between the rigid body and the wheel. k_t represents the stiffness of the tire [3]. The masses of the vehicle rigid body and the wheel are defined respectively by m_1 and m_2. x_1 and x_2 are the corresponding vertical displacements of the rigid body and the wheel, and the vertical velocities, v_1 and v_2, will be calculated by using x_1 and x_2. x_3 and v_{12} represents the displacement of

the contact point between the tire and the road, and the relative velocity across the suspension respectively [4].

The equation of motion of the quarter car model is divided into two equations for the sprung mass and the unsprung mass. The equation of motion of the sprung mass is defined as:

$$m_1\ddot{x}_1 = -k_s(x_1 - x_2) - c_s(\dot{x}_1 - \dot{x}_2) \quad \textbf{(2.1)}$$

and the equation of the unsprung mass is defined as:

$$m_2\ddot{x}_2 = k_s(x_1 - x_2) + c_s(\dot{x}_1 - \dot{x}_2) - k_t(x_2 - x_3) \quad \textbf{(2.2)}$$

1.1.2 Half Car Model

Half car model is a combination of two quarter car models, or half of the full car model. As shown in Figure 2, two individual unsprung masses are connected to a single rigid body of a half vehicle model. This model is also referred to as the bicycle model, since a bicycle uses two separate wheels and suspension systems which are connected to a single main frame.

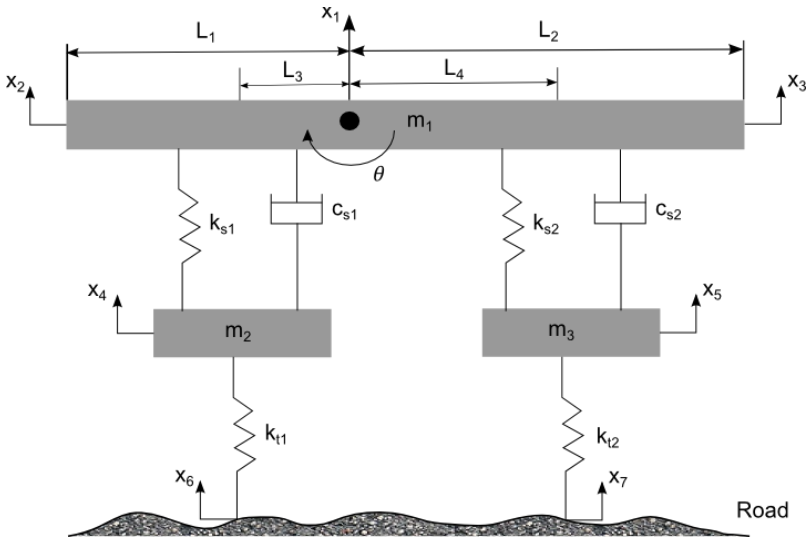

Figure 2: Half Car Model

Figure 2 represents a four degree of freedom half car model. The masses of the sprung mass of the model and two individual unsprung masses are defined as m_1, m_2, and m_3 respectively. There are two suspension systems which have one spring, k_s, and one damper, c_s between the sprung mass and

the unsprung masses. Two independent stiffness of tire, k_t, exist between the unsprung masses and the ground [3].

In this model, L_1 and L_2 are defined as distances between each end of the sprung mass and the center of gravity of the model along the longitudinal axis (x-axis), respectively. Therefore, the sum of L_1 and L_2 is the longitudinal length of the vehicle.

Furthermore, L_3 and L_4 represents distances between passenger seat locations and the center of gravity of the model along the longitudinal axis. Changing the location of the center of gravity will affect a pitching motion of the vehicle. Since the pitching motion is highly related to passenger ride comfort, it therefore means that the center of gravity affects ride comfort.

In order to obtain an accurate simulation result from the mathematical vehicle model and set up an efficient controller using the suspension system in the model, it is very important to measure accurate physical properties of the vehicle. If the properties change, the characteristics of the suspension systems and tire stiffness must be adjusted to make the suspension system suitable for the changed vehicle.

The equations of motion of the sprung mass and the unsprung masses are as follows [5][6][7]:

$$m_1\ddot{x}_1 = -c_{s1}(\dot{x}_2 - \dot{x}_4) - c_{s2}(\dot{x}_3 - \dot{x}_5) - k_{s1}(x_2 - x_4) - k_{s2}(x_3 - x_5) \quad \textbf{(2. 3)}$$

$$m_2\ddot{x}_4 = c_{s1}(\dot{x}_2 - \dot{x}_4) + k_{s1}(x_2 - x_4) - k_{t1}(x_4 - x_6) \quad \textbf{(2. 4)}$$

$$m_3\ddot{x}_5 = c_{s2}(\dot{x}_3 - \dot{x}_5) + k_{s2}(x_3 - x_5) - k_{t2}(x_5 - x_7) \quad \textbf{(2. 5)}$$

There is also another equation of motion for pitching:

$$I\ddot{\theta} = -l_3\big(c_{s1}(\dot{x}_2 - \dot{x}_4) + k_{s1}(x_2 - x_4)\big) + l_4\big(c_{s2}(\dot{x}_3 - \dot{x}_5) + k_{s2}(x_3 - x_5)\big) \quad \textbf{(2. 6)}$$

Unlike the equations of the motion of the quarter car model, the half car model now has an equation of pitch motion, which has the effect of the combination of two independent suspension systems. The angular acceleration, θ, in Equation (2. 6) causes a vertical acceleration at any location on the sprung mass via a correlation between a vertical and an angular acceleration, as follows:

$$a_{m1} = L\ddot{\theta} \quad \textbf{(2. 7)}$$

where a_{m1} is a vertical acceleration at the same location on the sprung mass and L is the longitudinal distance between the location and the axis of the rotation.

1.1.3 Full Car Model

Full car model is a combination of two half car models, or four quarter car models. As shown in Figure 3, four individual unsprung masses are connected to a single rigid body of a full vehicle model.

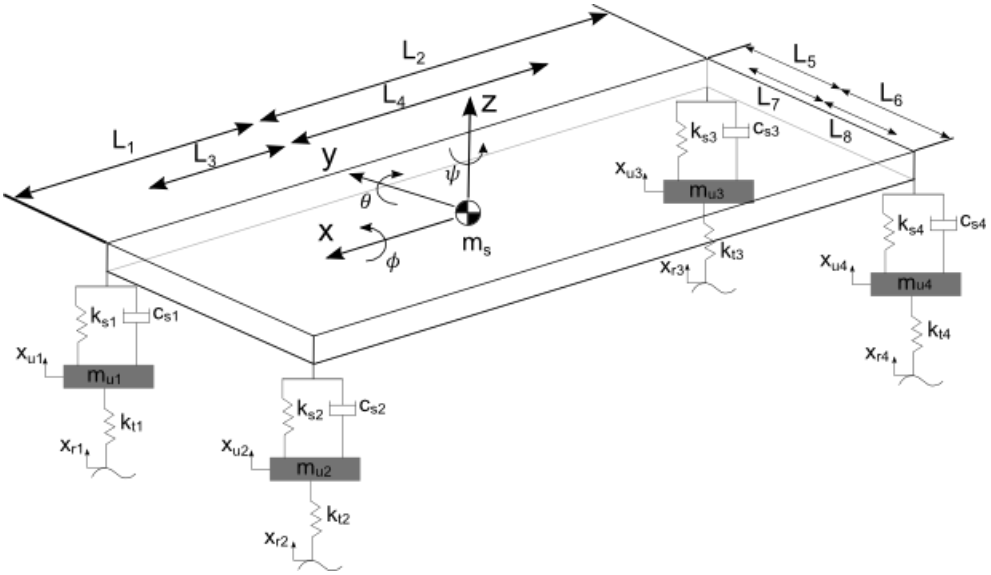

Figure 3: Full Car Model

Figure 3 represents a full car model with seven degrees of freedom. The mass of the sprung mass of the model and four individual unsprung masses are defined as m_s, m_{u1}, m_{u2}, m_{u3}, and m_{u4}, respectively. There are four suspension systems which have one spring, k_s, and one damper, c_s between the sprung mass and the unsprung masses. Four independent stiffness of tire, k_t, exist between the unsprung masses and the ground [3].

Unlike the half car model, the full car model considers the sprung mass as a rigid unit body so that only the mass of the sprung mass m_s exists. Therefore, it is now available to consider linear and angular motions about three axes. The four suspension systems connected to the sprung mass and each of the unsprung masses are located at each corner of the sprung mass.

In this model, L_1 and L_2 are defined as distances between each end of the sprung mass and the center of gravity of the model along the longitudinal axis (x-axis), respectively. Therefore, the sum of

L_1 and L_2 is the longitudinal length of the vehicle model. In addition, L_3 and L_4 represent distances between passenger seat locations and the center of gravity, along the same axis.

Furthermore, L_5 and L_6 represent distances between each end of the sprung mass and the center of gravity of the model along the lateral axis (y-axis). Therefore, the lateral length of the model is the sum of L_5 and L_6. L_7 and L_8 are defined as distances between passenger seat locations and the center of gravity of the model, along the same axis.

In the full car model, both pitching, θ, and rolling, ϕ, motions of the vehicle model in Figure 3 will be affected by a change in the location of the center of gravity. Additionally, even though L_7 and L_8 are not as far as L_3 and L_4 from the center of gravity due to the physical properties of the vehicle, the rolling motion is significant enough to cause vertical acceleration of each passenger seat, making it necessary to study when examining ride comfort.

The full car vehicle model uses four suspension systems and displays the roll, pitch and vertical (heave) motions of the model that result from the four suspension systems. Generally, the full car model covers whole dynamics of a vehicle so it is sufficient to use the full car model as an analytical method for ride comfort and road holding. Like the half car model, it is also important to set up the suspension systems and the tire stiffness based on the physical properties of the vehicle model to maximize its impact on vehicle control.

Below are the equations of motion of the sprung mass and the unsprung masses [8][9].

For the equation of motion of the sprung mass,

$$\begin{aligned} m_s\ddot{z} = &-m_s g - (k_{s1} + k_{s2} + k_{s3} + k_{s4})z - (c_{s1} + c_{s2} + c_{s3} + c_{s4})\,\dot{z} \\ &+\big(L_1(k_{s1} + k_{s2}) - L_2(k_{s3} + k_{s4})\big)\theta + \big(L_1(c_{s1} + c_{s2}) - L_2(c_{s3} + c_{s4})\big)\dot{\theta} \\ &+k_{s1}x_{u1} + c_{s1}\dot{x}_{u1} + k_{s2}x_{u2} + c_{s2}\,\dot{x}_{u2} + k_{s3}x_{u3} + c_{s3}\dot{x}_{u3} + k_{s4}x_{u4} \\ &+ c_{s4}\,\dot{x}_{u4} \end{aligned} \quad \textbf{(2. 8)}$$

For the equation of motion of the two angular accelerations along x and y axis of the chassis,

$$\begin{aligned} I_{xx}\ddot{\phi} = &-\left(\frac{L_5+L_6}{2}\right)^2(k_{s1}+k_{s2}+k_{s3}+k_{s4})\phi \\ &-\left(\frac{L_5+L_6}{2}\right)^2(c_{s1}+c_{s2}+c_{s3}+c_{s4})\dot{\phi} \\ &+\frac{L_5+L_6}{2}(k_{s1}x_{u1}+c_{s1}\dot{x}_{u1}-k_{s2}x_{u2}-c_{s2}\dot{x}_{u2}+k_{s3}x_{u3}+c_{s3}\dot{x}_{u3} \\ &\quad -k_{s4}x_{u4}-c_{s4}\dot{x}_{u4}) \end{aligned} \quad \textbf{(2. 9)}$$

$$\begin{aligned} I_{yy}\ddot{\theta} = &\left(L_1(k_{s1}+k_{s2})-L_2(k_{s3}+k_{s4})\right)z+\left(L_1(c_{s1}+c_{s2})-L_2(c_{s3}+c_{s4})\right)\dot{z} \\ &+\left(L_1^2(k_{s1}+k_{s2})-L_2^2(k_{s3}+k_{s4})\right)\theta+\left(L_1^2(c_{s1}+c_{s2})-L_2^2(c_{s3}+c_{s4})\right)\dot{\theta} \\ &+L_1k_{s1}x_{u1}+L_1c_{s1}\dot{x}_{u1}+L_1k_{s2}x_{u2}+L_1c_{s2}\dot{x}_{u2} \\ &-L_2k_{s3}x_{u3}-L_2c_{s3}\dot{x}_{u3}-L_2k_{s4}x_{u4}-L_2c_{s4}\dot{x}_{u4} \end{aligned} \quad \textbf{(2. 10)}$$

Derive the equations of motion of the unsprung masses as follows:

$$\begin{aligned} m_{u1}\ddot{x}_{u1} = &-m_{u1}g+k_{s1}z+c_{s1}\dot{z}-L_1k_{s1}\theta-L_1c_{s1}\dot{\theta} \\ &+\frac{L_5+L_6}{2}k_{s1}\phi+\frac{L_5+L_6}{2}c_{s1}\dot{\phi}-(k_{s1}+k_{t1})x_{u1} \\ &-c_{s1}\dot{x}_{u1}+k_{t1}x_{r1} \end{aligned} \quad \textbf{(2. 11)}$$

$$\begin{aligned} m_{u2}\ddot{x}_{u2} = &-m_{u2}g+k_{s2}z+c_{s2}\dot{z}-L_1k_{s2}\theta-L_1c_{s2}\dot{\theta} \\ &-\frac{L_5+L_6}{2}k_{s2}\phi-\frac{L_5+L_6}{2}c_{s2}\dot{\phi}-(k_{s2}+k_{t2})x_{u2} \\ &-c_{s2}\dot{x}_{u2}+k_{t2}x_{r2} \end{aligned} \quad \textbf{(2. 12)}$$

$$\begin{aligned} m_{u3}\ddot{x}_{u3} = &-m_{u3}g+k_{s3}z+c_{s3}\dot{z}+L_2k_{s3}\theta+L_2c_{s3}\dot{\theta} \\ &+\frac{L_5+L_6}{2}k_{s3}\phi+\frac{L_5+L_6}{2}c_{s3}\dot{\phi}-(k_{s3}+k_{t3})x_{u3} \\ &-c_{s3}\dot{x}_{u3}+k_{t3}x_{r3} \end{aligned} \quad \textbf{(2. 13)}$$

$$\begin{aligned} m_{u4}\ddot{x}_{u4} = &-m_{u4}g+k_{s4}z+c_{s4}\dot{z}+L_2k_{s4}\theta+L_2c_{s4}\dot{\theta} \\ &-\frac{L_5+L_6}{2}k_{s4}\phi-\frac{L_5+L_6}{2}c_{s4}\dot{\phi}-(k_{s4}+k_{t4})x_{u4} \\ &-c_{s4}\dot{x}_{u4}+k_{t4}x_{r4} \end{aligned} \quad \textbf{(2. 14)}$$

In the full car model, Equation (2. 9) and Equation (2. 10) have the moment of inertia (I_{xx} and I_{yy}), according to the corresponding axes, since rotation and twist of the sprung mass relates to the roll and pitch motions.

1.2 Suspension Systems

A suspension system is used to isolate road vibrations from passengers to improve ride comfort. In addition it needs to provide contact between the tire and road called road holding.

Its history begins with the passive suspension system. A passive suspension system only absorbs vibration energy and its characteristics cannot be modified to suit different road conditions. This deficit led to the development of semi-active and active suspension systems.

A semi-active suspension system consists of a spring and a damper, which can absorb vibration energy as the passive one does, but its damper's characteristics can vary depending on the road conditions. An active suspension can generate additional force to improve ride comfort and road holding. Active suspensions are more efficient in reducing vibration, it is, however, more expensive than a semi-active suspension system [2]. This section introduces passive, semi-active, and active suspension systems.

1.2.1 Passive Suspension Systems

Passive suspension systems are widely used to reduce and isolate road vibrations. A passive suspension system consists of a passive spring and a damper. The spring could be coil, leaf or air spring [10], [11]. There is either gas or oil fluid inside a damper, which goes through a constriction valve every time the damper moves. Each damper has its own damping coefficient. The characteristics of the fluid and restriction give the damper dynamic properties [11]. Classification of suspension systems is based on the damper's capability to change its damping coefficient.

As in Figure 1, a passive suspension system consists of one spring and one damper which are connected to the sprung mass and the unsprung mass of a vehicle. In a passive suspension, the characteristics of spring and damper are fixed and cannot vary to adapt to different road conditions.

1.2.2 Semi-Active Suspension Systems

A damper mechanism is different in a semi-active suspension system from that of the passive suspension system. Figure 4 depicts a typical semi-active suspension model. Unlike the passive

suspension systems, the damper characteristics can be changed in semi-active suspension systems [12] [13].

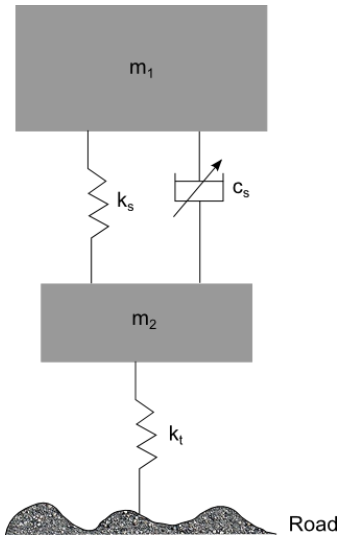

Figure 4: Semi-Active Suspension

The Magneto-Rheological damper is used the most in semi-active suspensions. The MR damper contains magnetic iron particles in a synthetic hydrocarbon base [14]. When applying a magnetic field using an electromagnetic coil, the particles will be placed in a straight line in a fibrous structure. Therefore, the viscosity of the fluid inside the damper will vary depending on the magnetic field it may encounter. With this mechanism, it is possible to change the damping characteristic of the suspension with respect to the road condition.

It costs less to build and maintain a semi-active suspension system than an active suspension. Furthermore, even though the suspension cannot generate additional forces to fully control the sprung mass motion, the suspension requires much lower energy compared with an active suspension.

1.2.3 Active Suspension Systems

An active suspension system consists of one actuator and could also include one spring and one damper. Therefore, unlike in the other suspension systems, an actuator generates additional force independently, in order to control the vertical movement of the sprung mass. By controlling it at each corner of a vehicle, the roll and pitch motion caused by independent vertical movement at each corner can be minimized more than any other suspension system.

Figure 5 represents a typical active suspension system. It depicts an additional actuator which can provide enough additional force to control the roll, pitch, and heave motions of the sprung mass, as well as the vertical motion of the unsprung mass [15] [16] .

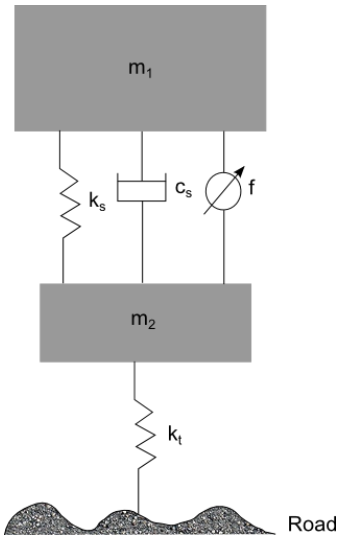

Figure 5: Active Suspension

While it needs more energy than other suspension systems, using the actuator in addition to the spring and the damper controls the entire vehicle's motion more than alternatives.

By controlling the three motions of the sprung mass, roll, pitch, and heave, it is possible to provide passengers better ride comfort as it is directly associated with their locations' vertical accelerations, and the vertical accelerations can be controlled by minimizing the roll, pitch, heave motions of the sprung mass.

In addition, controlling the vertical motion of the unsprung mass can provide better road holding. Since the actuator can generate force not only upward but also downward, the vertical acceleration of the unsprung mass can be controlled so that the unsprung mass is attached to the ground in any condition. This will offer drivers better driving experience by improving the road holding.

However, active suspension systems cost more than other suspension systems due to the additional actuator required to generate the force for controlling the motion of a vehicle.

Although active suspensions are technically available, due to their higher costs they are only available on limited commercial or special-duty vehicles.

1.3 Conventional Suspension Control Algorithms

Since the invention of semi-active and active suspension systems, many control algorithms have been developed to offer passengers better ride comfort and road holding. As an active suspension system can generate force in both vertical directions, these goals could be achieved far better than with the passive or semi-active suspension systems.

This section presents three different control algorithms. First, the skyhook control algorithm that controls the sprung mass provides better ride comfort. Second, the groundhook control algorithm that controls the unsprung mass improves road holding. Finally, the hybrid control algorithm that combines both the skyhook and groundhook control algorithms controls both the sprung mass and the unsprung mass to simultaneously obtain better ride comfort and road holding.

1.3.1 Skyhook Controller

The skyhook Control algorithm is a classical control strategy, which only considers driver and passenger ride comfort. The concept of this control algorithm is a sprung mass connected to an imaginary "sky" through one damper. The virtual reference point of the damper is considered the sky, with one damper between the sky and the sprung mass, and one spring between the sprung mass and the unsprung mass. Figure 6 depicts the skyhook controller [15] [17].

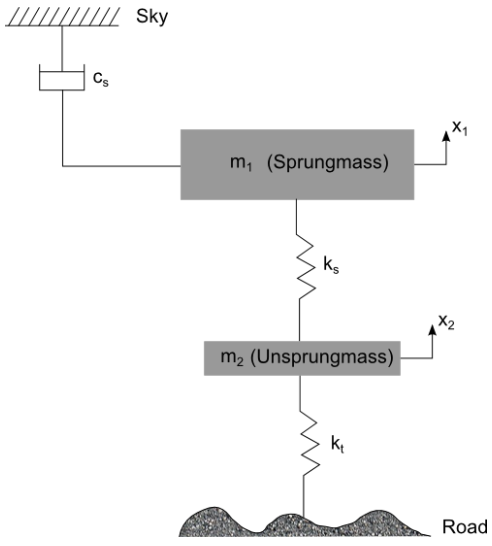

Figure 6: Skyhook Controller

The skyhook control algorithm can be classified into two different algorithms in terms of its continuity for controlling a suspension system [18].

One is the on-off skyhook control strategy. In the on-off skyhook controller, there are two damping variables used for two different conditions, by using velocities of the sprung mass and the unsprung mass. The following equations explain the conditions:

$$\dot{x}_1\dot{x}_{12} \geq 0 \quad \mathrm{c_s} = c_{max} \tag{2.15}$$

$$\dot{x}_1\dot{x}_{12} < 0 \quad \mathrm{c_s} = c_{min} \tag{2.16}$$

As in Equation (2. 15) and Equation (2. 16), if the product of the velocity of the sprung mass and the relative velocity between the sprung mass and the unsprung mass is positive or zero, it indicates that their velocities are in opposite directions, and the maximum damping coefficient will replace the damping coefficient. This also means that it will apply in the condition in which the suspension system is being expanded.

On the other hand, if the product of the velocities is negative, the minimum damping coefficient will adapt to the damping coefficient of the damper. This condition means that both the velocities are in the same direction. In other words, the suspension is being compressed in this condition.

The other skyhook controller is a continuous skyhook control algorithm. This algorithm can be considered an extension of the on-off skyhook control algorithm, which functions mostly for a continuous control with the semi-active suspension system, since the semi-active suspension system cannot generate force when the product of the velocities is negative [18]. Its equations, which express its condition for the application, are:

$$\dot{x}_1\dot{x}_{12} \geq 0 \quad \mathrm{c_s} = c_{sky} \tag{2.17}$$

$$\dot{x}_1\dot{x}_{12} < 0 \quad \mathrm{c_s} = 0 \tag{2.18}$$

In the continuous skyhook control algorithm, when the product of the velocity of the sprung mass and the relative velocity between the sprung mass and unsprung mass is positive or zero, the damping coefficient is assigned a constant damping coefficient of the skyhook controller. This applies when the suspension system is being expanded.

On the other hand, when the product of the velocities is negative, the damping coefficient will be zero. This applies only when the suspension system is being compressed.

After the damping coefficient is defined by the skyhook control algorithm, it is needed to be inserted into an equation of force of the suspension system, as defined in Equation (2. 19):

$$f = c_{sky}\dot{x}_1 \qquad \textbf{(2. 19)}$$

Equation (2. 19) generates the force needed for the suspension to provide better ride comfort.

Note: The skyhook controller only applies the damping force in order to reduce the vertical acceleration of the sprung mass, while taking away the damping force for the unsprung mass. Therefore, even though the vertical motion of the sprung mass will be minimized, the behavior of the unsprung mass can be as same as that without the skyhook control algorithm or poorer than that.

1.3.2 Groundhook Controller

Unlike the skyhook control algorithm, the groundhook control algorithm controls the vertical acceleration of the unsprung mass of a vehicle. This also means that the groundhook controller improves the property of a vehicle's road holding rather than ride comfort. There is a hypothetical "ground" attached to the end of the damper, and the damper is connected to the unsprung mass of a vehicle. One spring is connected between the sprung mass and the unsprung mass, as in the skyhook controller. Figure 7 depicts the groundhook controller configuration.

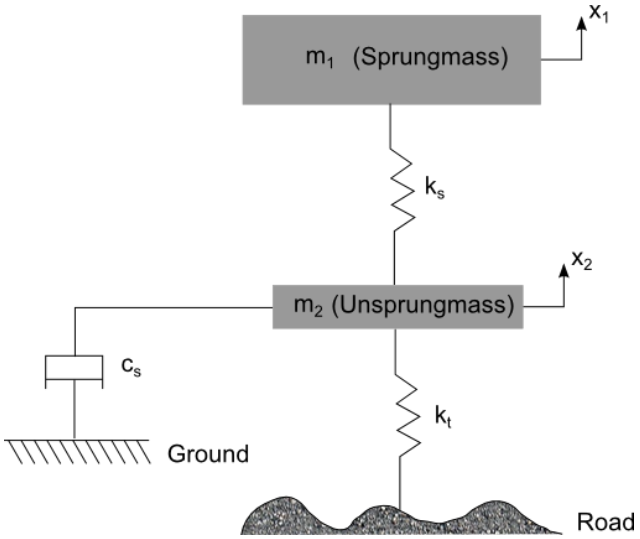

Figure 7: Groundhook Controller

Like the skyhook control algorithm, two cases can describe the groundhook control algorithm. When it is not considered with the semi-active suspension system, the groundhook controller is defined by:

$$\dot{x}_2\dot{x}_{21} \leq 0 \quad c_{ground} = c_{max} \tag{2.20}$$

$$\dot{x}_2\dot{x}_{21} > 0 \quad c_{ground} = c_{min} \tag{2.21}$$

In the groundhook Control algorithm, the velocity of the unsprung mass and the relative velocity between the unsprung mass and the sprung mass are considered in order to establish the condition. When the product of the velocities is negative or zero, the maximum damping coefficient will be assigned for the suspension system.

Alternatively, when the product of the velocities is positive, the damping coefficient of the suspension system will be replaced with the minimum damping coefficient.

In the case with the semi-active suspension system, Equation (2. 20) and Equation (2. 21) will be redefined as the following:

$$\dot{x}_2\dot{x}_{21} \leq 0 \quad c_{ground} = c_{ground} \tag{2.22}$$

$$\dot{x}_2\dot{x}_{21} > 0 \quad c_{ground} = 0 \tag{2.23}$$

Due to the characteristics of the semi-active suspension system, when the product of the velocities is positive, the damping coefficient will be zero.

After acquiring the assigned damping coefficient, the necessary force to compensate vibration can be found by using equation of force of the suspension system as shown in Equation (2. 24):

$$f = c_{ground}\dot{x}_2 \tag{2.24}$$

The groundhook controller can reduce the vertical acceleration of the unsprung mass, which indicates that road holding of the wheel will subsequently improve.

The groundhook algorithm controls the vertical motion of the unsprung mass, not that of the sprung mass. Therefore, the unsprung mass will be attached to the ground using this control algorithm. However, there is a damper between the sprung mass and the unsprung mass, while the hypothetical damper is connected between the unsprung mass and the ground. As a result, there is still a stabilizing effect on the vertical motion of the sprung mass as well as the unsprung mass.

1.3.3 Hybrid Controller

The hybrid control algorithm is an integration of the skyhook and groundhook controllers. Since the skyhook and groundhook controller can only focus on the vertical motion of one of the sprung mass and the unsprung mass of a vehicle, the hybrid control algorithm functions to control both simultaneously.

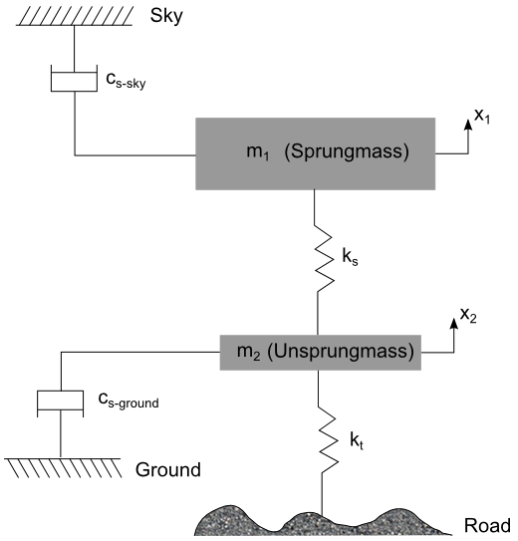

Figure 8: Hybrid Controller

The mathematical model for the hybrid controller is defined as:

$$f_{hybrid} = \alpha f_{sky} + (1 - \alpha) f_{ground} \quad \textbf{(2. 25)}$$

where

$$f_{sky} = c_{sky} \dot{x}_1 \quad \textbf{(2. 26)}$$

and

$$f_{ground} = c_{ground} \dot{x}_2 \quad \textbf{(2. 27)}$$

Each damping coefficient for the skyhook and groundhook controllers is defined as:

$$c_{sky} = \begin{cases} c_{max} & when\ \dot{x}_1 \dot{x}_{12} \geq 0 \\ c_{min} & when\ \dot{x}_1 \dot{x}_{12} < 0 \end{cases} \quad \textbf{(2. 28)}$$

and

$$c_{ground} = \begin{cases} c_{max} & when\ \dot{x}_2\dot{x}_{21} \leq 0 \\ c_{min} & when\ \dot{x}_2\dot{x}_{21} > 0 \end{cases} \quad \textbf{(2. 29)}$$

In the hybrid controller, it is possible to adjust both the skyhook and groundhook control algorithms by changing the variable, α. Therefore, the hybrid controller can switch the weight for each of the skyhook and groundhook controllers based on the road condition. If the road condition is very rough, the hybrid controller can put more weight on the groundhook controller, i.e. α is almost zero in this case, so that it can control the unsprung mass more than the sprung mass, in order to keep the wheel in constant contact with the ground for better road holding. Alternatively, on the smooth road, the hybrid controller can put more weight on the skyhook, i.e. α is almost 1 in this case, so that it can control the sprung mass more than the unsprung mass, in order to provide better ride comfort.

Chapter 2
Modelling and Control of Suspension Systems

2.1 Suspension and Road Profile Modelling

2.1.1 Damper Characteristics (Mapping and Inverse-Mapping)

In order to utilize a suspension system for controlling both a sprung mass and an unsprung mass, it is necessary to know the dynamics of a suspension system. Furthermore, since a control for a semi-active suspension system will be developed in this thesis, the characteristics of the damper are required.

STS Cadillac vehicle model used in this thesis uses a semi-active suspension system, which consists of a magneto-rheological damper, aka MR damper. This MR damper is filled with magneto-rheological fluid and the fluid is controlled by a magnetic field, as explained in Chapter 1. This type of suspension system is effective, especially with semi-active suspension systems.

The semi-active suspension system with MR damper generates a force that can be estimated by [19]:

$$f_d = -m_2\ddot{x}_2 + k_s(x_1 - x_2) - k_t(x_2 - x_3) \quad \textbf{(3. 1)}$$

where m_2 is a mass of the unsprung mass. x_1, x_2, and x_3 are vertical displacements of the sprung mass, unsprung mass, and tire, respectively. k_s and k_t are a spring and tire as shown in Figure 1.

While the damper generates force, the input to the damper has to be a current i [A] rather than the force f_d [N]. Therefore, the output from a control algorithm also has to be the current i so that the damper can generate necessary force, depending on the current.

In order to define the characteristics of the damper, an experiment on the front-left suspension system used the whole vehicle model to obtain the characteristics of the damper, meaning the damper was not tested independently for this experiment.

It is also necessary to know the suspension velocity in order to obtain the relationship between the damping force and the suspension velocity, since the damping force varies according to the suspension velocity at a constant current.

In this experiment, the current was set to be from 0 A to 4.2 A, and the vehicle model had a harsh pitching motion at each current so that the suspension velocity is distinct enough to be compared [19].

2.1.1.1 Mapping

The process to obtain the right damping force by using the current and the suspension velocity is called “Mapping.” It is possible to map both the current and the suspension velocity into the damping force with the data from the experiment, which was executed on the front-left suspension system of the Cadillac STS vehicle model.

There are several methods to map the characteristics of the damper. In this thesis, a look-up table method is used as a fast and effective way to adopt the characteristics into a control algorithm

Since the data points of the suspension system are not sufficient for mapping, it is important to consider if interpolated points with the actual data points are smooth enough to use prior to adding them into the control algorithm.

Figure 9 represents the data points collected in the experiment for mapping, a spline interpolated line, and a piecewise cubic hermite interpolated line, by using the data points. In Figure 9, it seems that both interpolated lines have similarities. However, Figure 10 shows that when zooming into several specific areas of Figure 9, those lines are not identical.

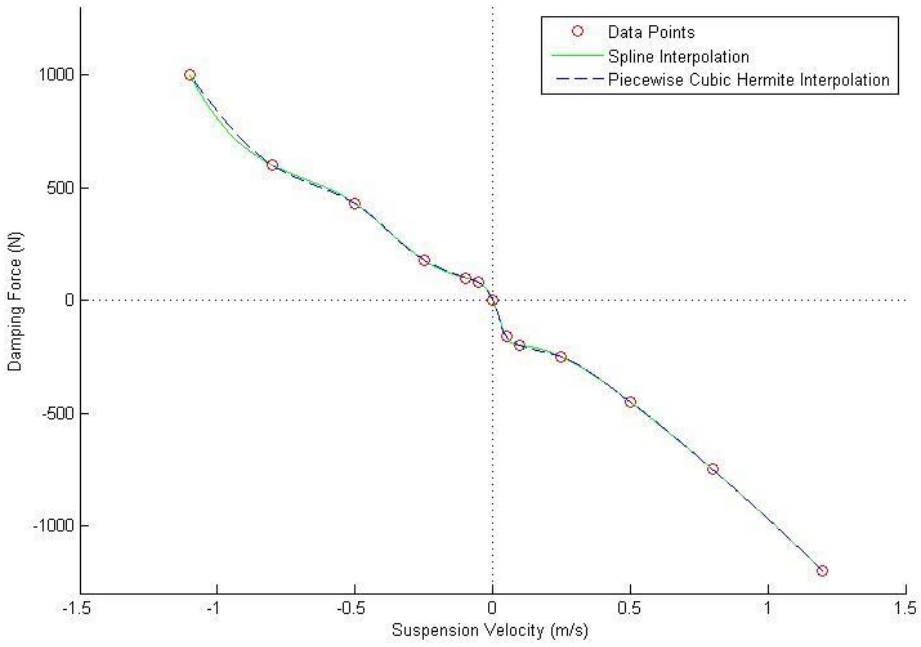

Figure 9: Spline vs Piecewise Cubic Hermite Interpolation

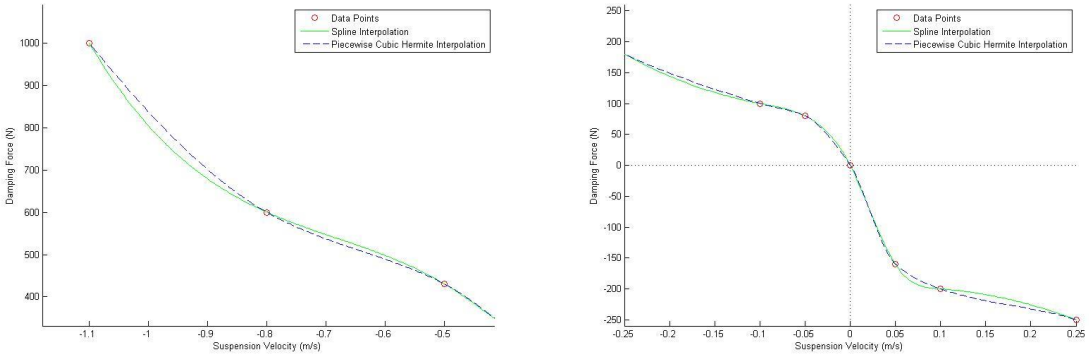

Figure 10: Zoomed-In Figures from Figure 9

Even though it is not possible to expect the interpolated points as actual characteristic points of the damper, using a smoother interpolated line would help the damper behave in a closer way to its own natural way. If a line has more sloped curves, the damper needs to behave more harshly than when the line has smoother curves so that the vehicle could be controlled less effectively with a more sloped curved line.

After several data points for the characteristics of the damping are acquired at different currents, the entire characteristics of the damper can be obtained in order to use it in the control algorithm. Figure 11 represents the characteristic curves of the damper obtained at different currents.

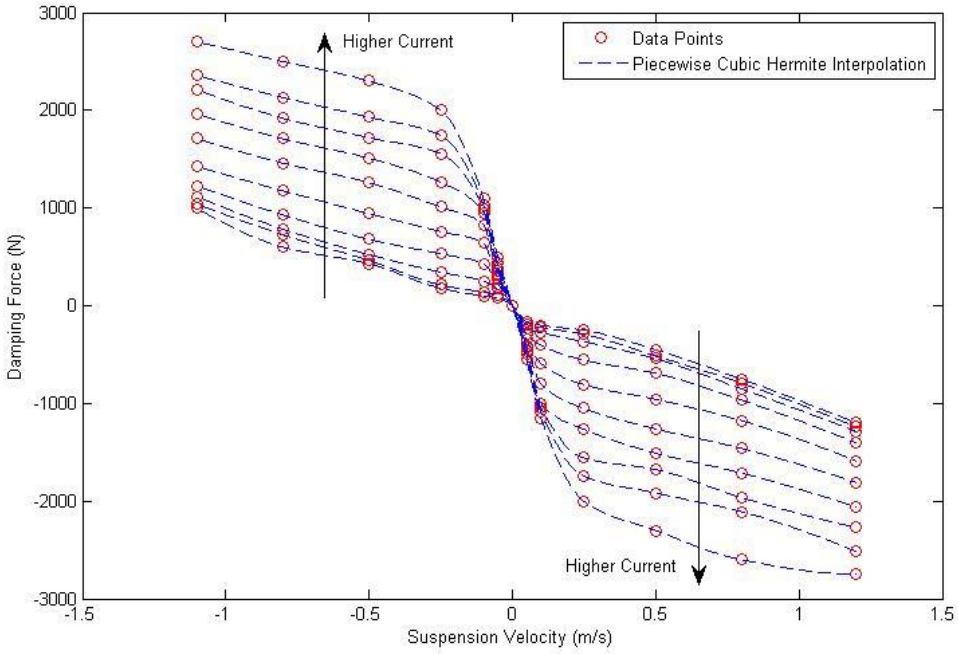

Figure 11: Damping Characteristics Curves

As shown in Figure 11, most of curves have the same shape, but with different slopes and different absolute values of the damping force at each current value. At the same suspension velocity, the damper can generate a more powerful force with higher current. In other words, the damper can generate more powerful force with higher suspension velocity at the same current level. Note that this damping characteristic model does not include hysteretic damping characteristics.

Figure 12 depicts the characteristics of the damper in a 3D map.

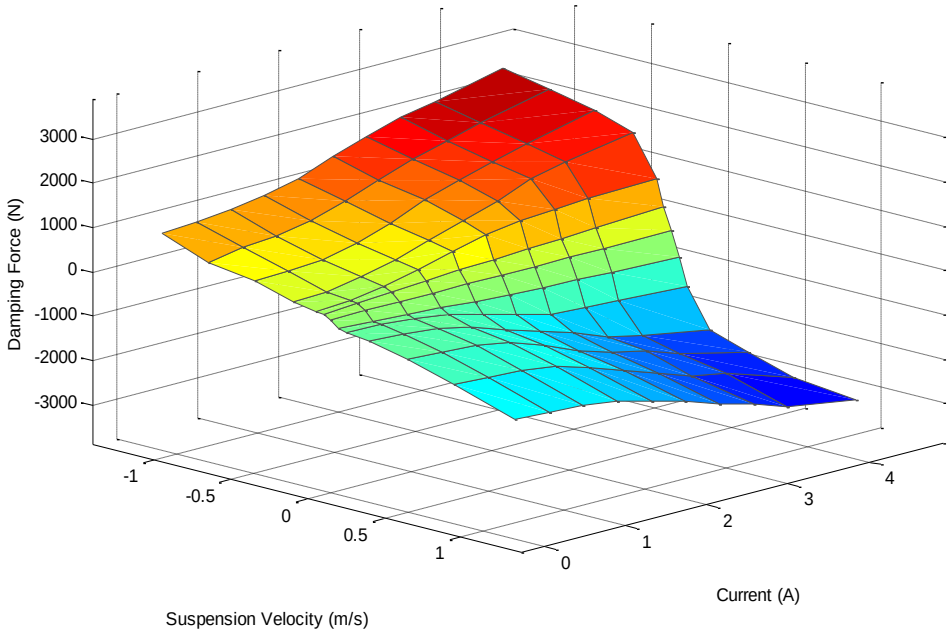

Figure 12: Damping Characteristics (3D Map)

2.1.1.2 Inverse-Mapping

In order to acquire the present current converted by the damping force of the damper, it is necessary to use the inverse-mapping of the characteristics of the damper by using the damping force and the suspension velocity at each moment.

Figure 13 shows the inverse-mapping of the characteristics of the damper. By knowing the damping force and the suspension velocity of the damper, the current required to generate the accurate amount of damping force from the controller to the damper can be calculated.

Figure 14 depicts inverse-mapping in three dimensions.

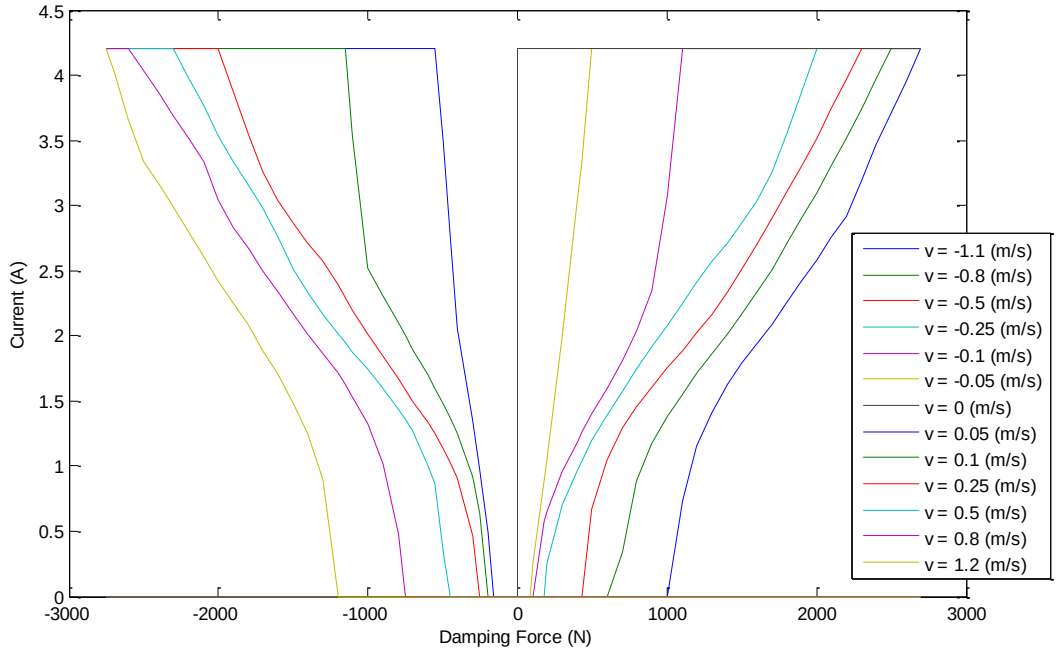

Figure 13: Inverse-Mapping of the Characteristics of the Damper

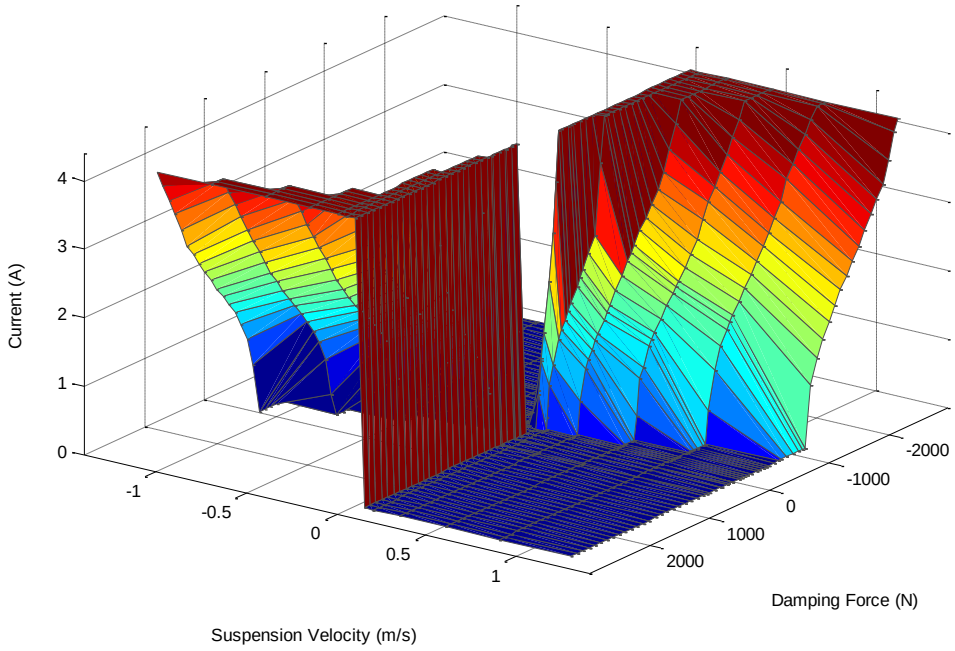

Figure 14: Inverse-Mapping of the Characteristics of the Damper (3D Map)

2.1.2 Bump Configuration

For a practical experiment, a rubber bump will be used for a test using Cadillac STS vehicle model. Figure 15 depicts the shape of the bump.

Figure 15: A Rubber-Made Bump

Table 1 represents the bump's specifications:

Table 1: A bump's Specification

Height	0.05715 m
Width	0.3048 m
Length	1.8288 m

The bump will be set up on the road in a stable manner and the test vehicle will run over the bump at the constant speed of 30 kph.

CarSim software was used to simulate the response of the vehicle with respect to the bump. Mathematically, it is possible to represent the bump using the following equation [20]:

$$r(t) = a(1 - \cos(8\pi t))/2 \qquad \textbf{(3. 2)}$$

where a is the amplitude of the bump, which is 0.05715 m, and t denotes the time. In order to relate X coordinate of the road to Equation (3. 2), t is replaced with x, which is X coordinate of the road, and Equation (3. 2) is modified as the following, with a condition for x:

$$r(x) = \begin{cases} a(1 - \cos(6.7\pi x))/2 & if \quad 0.7 \text{ m} < x < 1 \text{ m} \\ 0 & otherwise \end{cases} \qquad \textbf{(3. 3)}$$

Figure 16 depicts the bump modeled for the simulation.

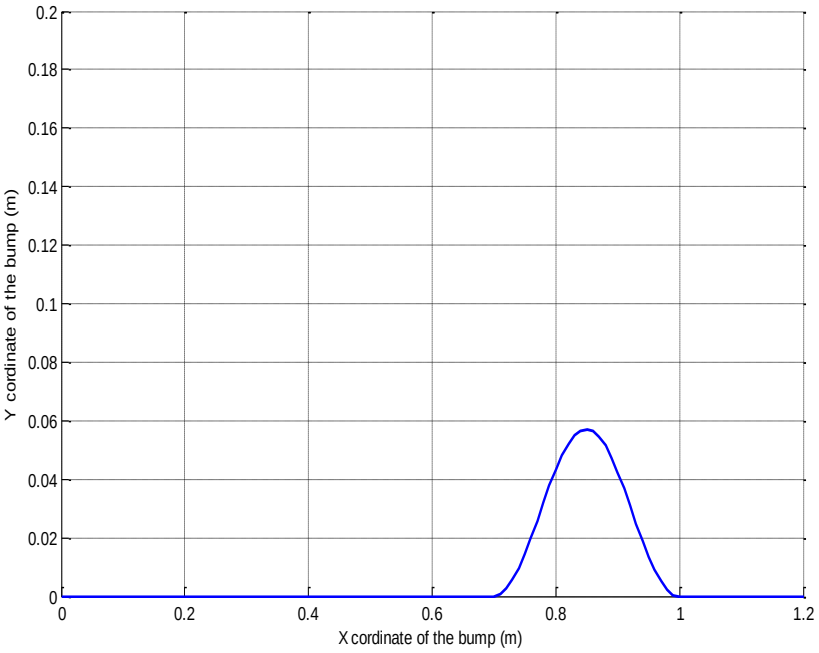

Figure 16: Configuration of the Bump

2.1.3 Random Road Input

In order to test the vehicle's behavior on a hypothetical road in simulation, it is important to establish a road model similar to a practical road. Sine waves, step function, and triangular waves have been only used to express the excitation from the ground. However, this method is not valid for studying the response of the vehicle model in a lifelike random road condition [21].

Even though it is impossible to express the actual road condition in a deterministic manner, it is feasible to describe some properties of a random road statistically. For instance, the mean or mean-square value of a random function can be defined by averaging. In addition, the frequency of the function can be also expressed by Fourier Transform.

When the statistical property of some part of the road is considered to be equal to that of another part of the road, the road profile is defined as stationary. In addition, when the statistical property of the road on a plane is considered equal to that of the road on another parallel plane, the road profile is described as ergodic. If the random road profile is stationary and ergodic, it is significantly convenient to model the random road profile.

For the random road modelling, the mean-square value of the amplitude of the random road profile is the most important factor to consider. To obtain an equation of the mean-square value of the component $\bar{z}_n{}^2$, the harmonic component $z_n(x)$ with amplitude Z_n and wavelength l_{wn} can be defined as:

$$z_n(x) = Z_n \sin\left(\frac{2\pi x}{l_{wn}}\right) = Z_n sin\Omega_n x \qquad \textbf{(3. 4)}$$

where $\Omega_n = \frac{2\pi}{l_{wn}}$, which is the circular spatial frequency of the harmonic component (rad/m).

Therefore, the mean-square value of the component $\bar{z}_n{}^2$ is

$$\overline{z}_n^2 = \frac{1}{l_{wn}} \int_0^{l_{wn}} \left[Z_n \sin\left(\frac{2\pi x}{l_{wn}}\right)\right]^2 dx = \frac{Z_n^2}{2} \qquad \textbf{(3. 5)}$$

By letting $S(n\Omega_0)$ be the power spectral density of the mean-square value in the interval $\Delta\Omega$ at frequency $n\Omega_0$, the following relation can be obtained:

$$S(n\Omega_0)\Delta\Omega = \frac{Z_n^2}{2} = \overline{z}_n^2 \qquad \textbf{(3. 6)}$$

The power spectral density of the mean-square value, therefore, can be rewritten as:

$$S(n\Omega_0) = \frac{Z_n^2}{2\Delta\Omega} = \frac{\overline{z}_n^2}{\Delta\Omega} \qquad \textbf{(3. 7)}$$

By using this relationship between the power spectral density and the circular spatial frequency, the relationship for the random road profile can be defined as:

$$S_g(\Omega) = C_{sp}\Omega^{-N} \qquad \textbf{(3. 8)}$$

where $\boldsymbol{S_g(\Omega)}$ is the power spectral density function of the elevation of the surface profile, and $\boldsymbol{C_{sp}}$ and $\boldsymbol{N}$ are the constants as shown in Table 2.

Table 2: Values of C_{sp} and N for Power Spectral Density Functions for Various Surfaces

No.	Description	N	C_{sp}
1	Smooth runway	3.8	4.3×10^{-11}
2	Rough runway	2.1	8.1×10^{-6}
3	Smooth highway	2.1	4.8×10^{-7}
4	Highway with gravel	2.1	4.4×10^{-6}
5	Pasture	1.6	3.0×10^{-4}
6	Plowed field	1.6	6.5×10^{-4}

Many organizations attempted to classify the irregularity of a random road profile. This thesis uses the one which the International Organization for Standardization (ISO) proposed (classes A-H) based on the power spectral density [21] [22].

The classification by ISO approximated the relationships between the power spectral density $S_g(\Omega)$ and the spatial frequency Ω for different classes of the random road profile using two straight lines with different Ns, 1.5 and 2.0, on a log-log scale. The equations for the relationships are expressed as:

$$S_g(\Omega) = \begin{cases} S_g(\Omega_0)\left(\frac{\Omega}{\Omega_0}\right)^{-2.0} & for\ \Omega \le \Omega_0 = \frac{1}{2\pi}\ \text{cycles/m} \\ S_g(\Omega_0)\left(\frac{\Omega}{\Omega_0}\right)^{-1.5} & for\ \Omega > \Omega_0 = \frac{1}{2\pi}\ \text{cycles/m} \end{cases} \quad \textbf{(3.9)}$$

Table 3 represents the range of the values of $S_g(\Omega)$ at a spatial frequency $\Omega_0 = \frac{1}{2\pi}$ cycles/m for different classes of road. Class B (conditionally a good road) is used for the simulation of the vehicle model as the actual road is in good condition.

Table 3: Classification of Road Roughness Proposed by ISO

	Degree of roughness $S_g(\Omega_0)$, 10^{-6} $m^2/cycles/m$	
Road class	**Range**	**Geometric mean**
A (very good)	<8	4
B (good)	8-32	16
C (average)	32-128	64
D (poor)	128-512	256
E (very poor)	512-2048	1024
F	2048-8192	4096
G	8192-32,768	16384
H	>32,768	

Class B random road profile is depicted in Figure 17.

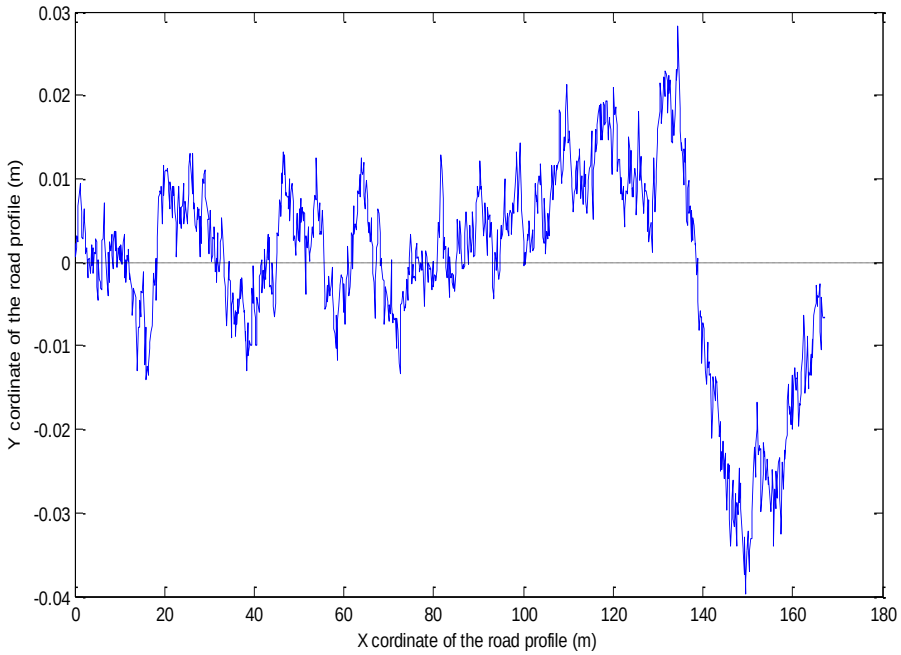

Figure 17: Class B Random Road Profile

Since the vibration of the random road and the vehicle model will be considered to be in the time domain, the spatial frequency Ω (cycles/m) should be converted to **Hz** (cycles/s) using the following equation:

$$f(\mathbf{Hz}) = \Omega V \quad \textbf{(3. 10)}$$

where V is the speed of the vehicle model in m/s.

In addition, the power spectral density of the random road profile (m^2/cycles/m) should be converted for the time domain ($\mathrm{m}^2/\mathbf{Hz}$):

$$S_g(f) = \frac{S_g(\Omega)}{V} \quad \textbf{(3. 11)}$$

2.2 Suspension Control

By using the suspension system, it is possible to control the vertical acceleration of the sprung mass of the vehicle, which directly relates to the passenger's ride comfort.

This section studies three different suspension systems and the vehicle's different responses.

Before studying the differences of the vehicle's responses, it is necessary to have an accurate mathematical model for the vehicle, including the suspension system. CarSim software tool is used to create the vehicle representation. In CarSim, there are data sheets of every component of the vehicle model, making it possible to simulate the model to obtain relatively accurate responses to the bump and the random road profile.

By using CarSim software, the algorithm for the suspension system is the only subject to model to control the motion of the vehicle model.

2.2.1 Vehicle Configuration

After testing the real vehicle model and obtaining the requisite data sheets, they are implemented in CarSim software to represent the vehicle in simulation. The mathematical model for the suspension system, in addition to the vehicle's data sheets, is required for the response of the vehicle on some road conditions.

In order to build the suspension system using an ordinary vehicle control algorithm, that is, the skyhook controller, it is required to adopt the skyhook control algorithm for the full car model to control the motion of the entire vehicle.

The idea of the skyhook control algorithm, which is explained in Chapter 1, is used with the full car model which is also described in Chapter 1. In order to implement the skyhook control algorithm, the maximum and minimum values of the damping coefficients of the damper which are used in the skyhook controller must be set up. In this case, the maximum and minimum damping coefficients are obtained from the data sheet of the damper of the vehicle model and the minimum damping coefficient is set to zero when the suspension system is semi-active.

Figure 18 depicts the diagram of the controller. After the sensor detects the vehicle's motion in real time, the sensors send the data of the vehicle's motion such as pitch, roll rates, and vertical acceleration to the controller, which is the skyhook controller, in this case. The controller generates a current as an input to the actuator or the damper in the suspension system, which is the damper, generates a force based on the current so that the suspension can control the vehicle model by itself. Details of this will be discussed in Chapter 4.

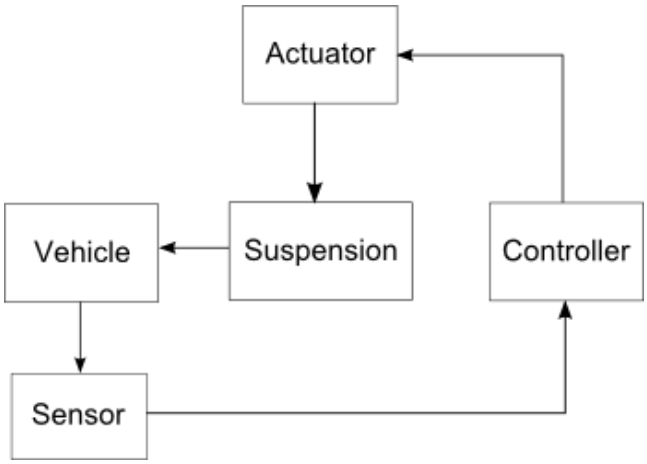

Figure 18: Diagram of Control System

2.2.2 Pitch, Roll Rates, and Vertical Acceleration at C.G. and Passenger Seat

The data of pitch and roll rates, and vertical velocity at the center of gravity of the vehicle model can be obtained via simulation in CarSim software. Since the skyhook control algorithm works for each corner of the vehicle and does not focus on the motion of the center of gravity, it is necessary to estimate the vertical velocities of the sprung mass and the unsprung mass of the vehicle model. With the values of roll and pitch rates, and vertical velocity at the center of gravity, estimate the vertical velocities at each corner of the vehicle model in SAE coordinate system using Equation (3. 12):

$$v = \begin{Bmatrix} v_1 \\ v_2 \\ v_3 \\ v_4 \end{Bmatrix} = \begin{Bmatrix} v_{CG} - \frac{(L_5 + L_6)}{2}\dot{\phi} - L_1\dot{\theta} \\ v_{CG} + \frac{(L_5 + L_6)}{2}\dot{\phi} - L_1\dot{\theta} \\ v_{CG} - \frac{(L_5 + L_6)}{2}\dot{\phi} + L_2\dot{\theta} \\ v_{CG} + \frac{(L_5 + L_6)}{2}\dot{\phi} + L_2\dot{\theta} \end{Bmatrix} \quad \textbf{(3. 12)}$$

The skyhook control algorithm uses Equation (3. 12) to estimate the vertical velocity at each corner, so that it can control the vertical motion of the sprung mass at each corner. Note that the skyhook controller is not the controller affecting the vertical motion at a passenger seat location. Therefore, there is a drawback that the controller affects the vertical motion of any passenger seat indirectly. In addition, CarSim software can yield the vertical velocity of the unsprung mass.

In the next subsection, the passive, semi-active, and active suspension systems are simulated with the skyhook control algorithm to examine the vertical acceleration of a passenger seat with the controller.

2.2.3 Results

Figure 19 depicts the vertical acceleration at the front-left passenger seat location. The passive suspension system shows more oscillations than other systems. Even though the skyhook controller with a semi-active suspension system shows higher peak values of the vertical acceleration when the vehicle model's front wheels hit the bump, the controller shows lower peaks and less oscillation after the moment when the rear wheels hit the bump. The skyhook controller with the active suspension system shows smaller peak values of the vertical acceleration generally and less oscillation than any other systems.

Table 4 depicts the RMS (Root Mean Square) of the vertical accelerations of each system. The skyhook with the active suspension system shows the best performance, as expected. Since the skyhook control algorithm only works at each corner of the vehicle model, not at the passengers' actual seat location, the RMS values do not seem to be affected significantly by the controller.

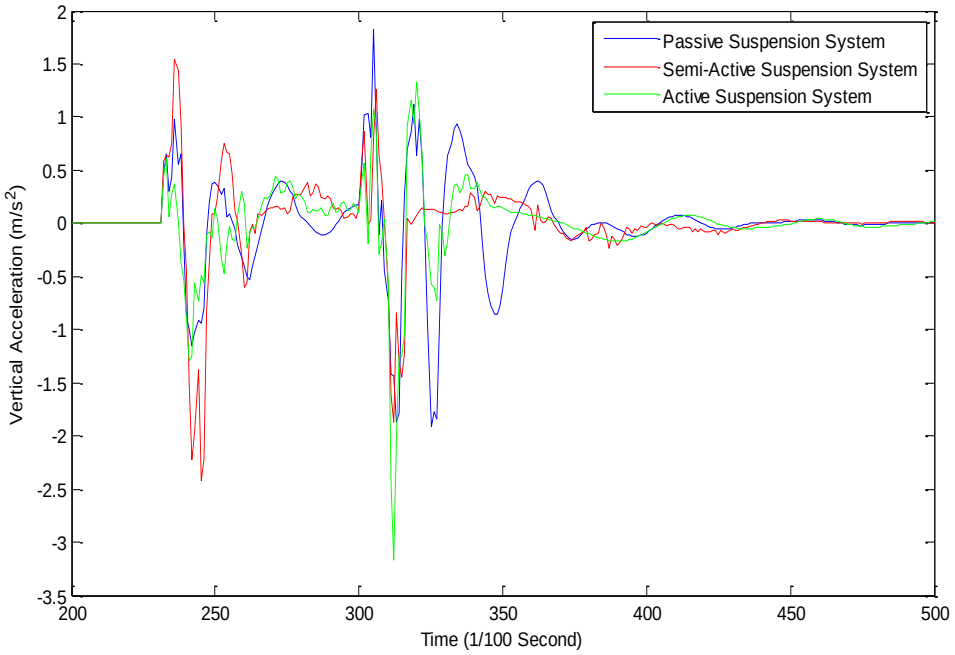

Figure 19: Vertical Acceleration at the Front Left Passenger Seat Location with Skyhook Control Algorithm (Different Suspension Systems)

Table 4: RMS of the Vertical Acceleration at the Front Left Passenger Seat Location with Skyhook Control Algorithm (Different Suspension Systems)

	RMS	Difference (Relative to Passive)
Passive	0.2413	0 %
Skyhook (Semi-Active)	0.2338	3.11 %
Skyhook (Active)	0.2327	3.56 %

Figure 20 depicts the vertical acceleration at the rear-left passenger seat location. Similar to the vertical acceleration at the front-left passenger seat location, the passive suspension system shows more oscillation than other systems. In addition, the skyhook controller with the semi-active suspension system prevents the oscillation, but it still has a few higher peak values. The skyhook controller with the active suspension system provides less oscillations as well as lower peaks, compared to the other systems generally.

RMS of the vertical accelerations of each system is shown in Table 5. At the front-left passenger seat location, the skyhook with the active suspension system shows the best performance. Since the

distance between the center of gravity of the vehicle model and the rear-left passenger seat location is longer than between the center of gravity and the front-left passenger seat location, the effect on the rear-left passenger seat location seems to be more significant than that on the front-left passenger seat location.

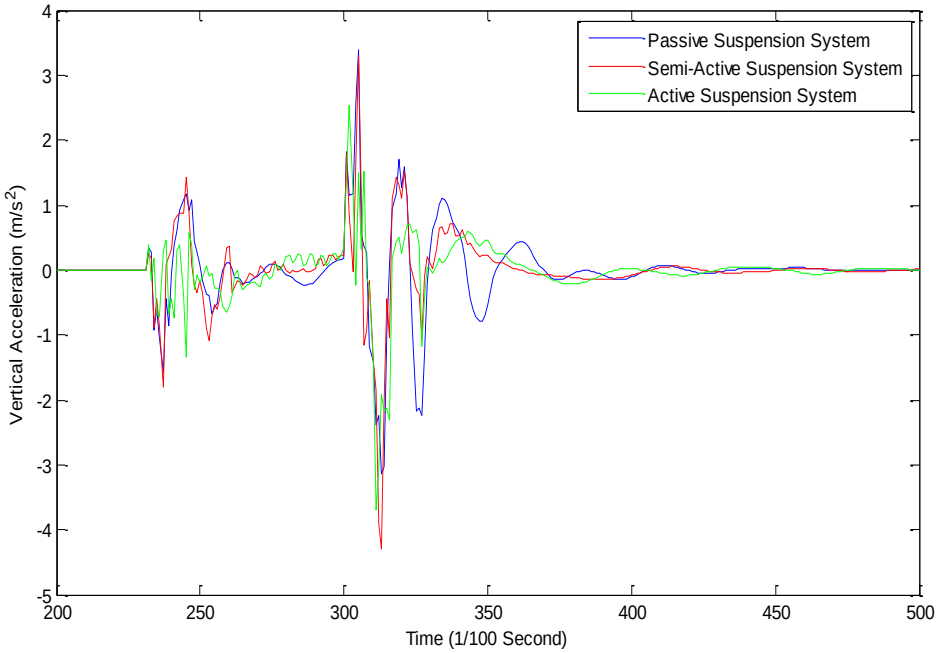

Figure 20: Vertical Acceleration at the Rear Left Passenger Seat Location with Skyhook Control Algorithm (Different Suspension Systems)

Table 5: RMS of the Vertical Acceleration at the Rear Left Passenger Seat Location with Skyhook Control Algorithm (Different Suspension Systems)

	RMS	Difference (Relative to Passive)
Passive	0.3365	0 %
Skyhook (Semi-Active)	0.3130	6.98 %
Skyhook (Active)	0.2741	18.54 %

Figure 21 depicts the vertical acceleration at a farther location. Similar to the vertical accelerations at the front-left and rear-left passenger seat locations, the skyhook controller with the passive suspension system shows bigger oscillation than other systems. In addition, the skyhook controller with the semi-active suspension system prevents the oscillation, but it still has similar peak values as that with the passive suspension system. Lastly, the skyhook controller with the active suspension system provides some high frequency oscillation temporarily. However, it reduces the peak values of the vertical acceleration.

RMS of the vertical accelerations of each system is described in Table 6. Similar to Table 5 and Table 6, the skyhook controller with the active suspension system has the best performance. The effect on this location is bigger than any other locations especially when the skyhook controller with the semi-active suspension system is applied.

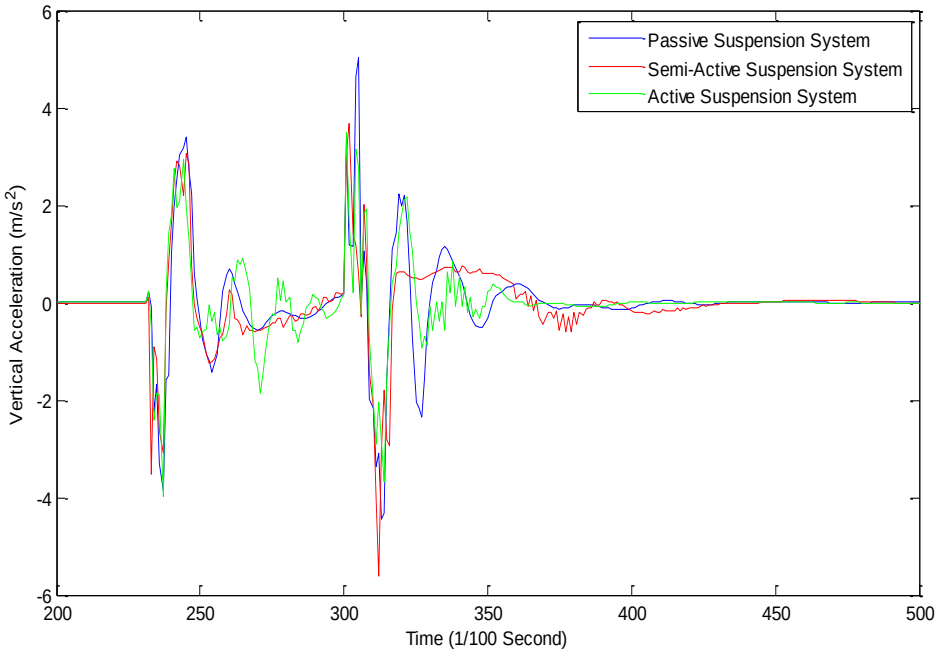

Figure 21: Vertical Acceleration at the Further Location with Skyhook Control Algorithm (Different Suspension Systems)

Table 6: RMS of the Vertical Acceleration at the Further Location with Skyhook Control Algorithm (Different Suspension Systems)

	RMS	Difference (Relative to Passive)
Passive	0.5361	0 %
Skyhook (Semi-Active)	0.4756	11.28 %
Skyhook (Active)	0.4361	18.65 %

Chapter 3
Localized-Based Suspension Controller

3.1 Vehicle Configuration

In this Chapter, the full car model is used for simulation with the passive, semi-active, and active suspension systems as in Chapter 2. The reason why the full car model is chosen is to obtain relatively accurate simulation results before an actual experiment. Compared to the passive suspension system, a new control algorithm, which is a localized-based control algorithm, is developed and simulated by using the semi-active and active suspension systems.

The same vehicle model as in Chapter 2 is used in this chapter, still using CarSim software. Instead of the skyhook controller, the localized-based controller is applied to control the vertical motion of the sprung mass. The next section discusses the method to find the vertical acceleration at a passenger seat location.

3.2 Target (Cost) Function for Ride Comfort

HCC (Holistic Corner Control) is an objective-function-based optimization algorithm [23]. This algorithm is based on force elements, which are applied to the tires of a vehicle.

$$P = \frac{1}{2}\left\{\left(E - A_f \delta f\right)^T W_E \left(E - A_f \delta f\right) + \delta f^T W_{df} \delta f + (f + \delta f)^T W_f (f + \delta f)\right\} \qquad (4.1)$$

where $\delta f = \left\{\delta f_{x1}, \delta f_{y1}, \delta f_{x2}, \delta f_{y2}, \delta f_{x3}, \delta f_{y3}, \delta f_{x4}, \delta f_{y4}\right\}^T$.

It has three terms to optimize three objectives. The first is to minimize errors between desired and actual forces at the center of gravity. The second is to minimize amplitudes of the control adjustment. The last is to maximize tire reserves for stabilizing a vehicle.

After replacing the tire forces with the vertical forces, which apply to each corner of the vehicle model in the objective function, and removing the third term, the objective function will be:

$$P = \frac{1}{2}\left\{\left(E - A_f \delta f_z\right)^T W_E \left(E - A_f \delta f_z\right) + \delta f_z^T W_{df} \delta f_z\right\} \qquad (4.2)$$

where $\delta f_z = \{\delta f_{z1}, \delta f_{z2}, \delta f_{z3}, \delta f_{z4}\}^T$.

By taking a derivative, the objective function should be zero to get an optimum solution:

$$\frac{\partial P}{\partial \delta f_z} = 0 \qquad (4.3)$$

Therefore,

$$\frac{\partial P}{\partial \delta f_z} = -A_f^T(W_E E) + \left(A_f^T W_E\right) A_f \delta f_z + W_{df} \delta f_z = 0 \qquad (4.4)$$

By rearranging Equation (4. 4) for δf_z to obtain the closed form solution of the objective function,

$$\delta f_z = \left[W_{df} + \left(A_f^T W_E\right) A_f\right]^{-1} \left[A_f^T (W_E E)\right] \qquad (4.5)$$

If the control algorithm for each suspension system at each corner is only considered, the Jacobian matrix, A_f, in Equation (4. 5) will be constant when taking a derivative with f_z, which means:

$$A_f = Jac_{4\times 4} = \begin{bmatrix} 1 & 0 & 0 & 0 \\ 0 & 1 & 0 & 0 \\ 0 & 0 & 1 & 0 \\ 0 & 0 & 0 & 1 \end{bmatrix} \qquad (4.6)$$

In this case, the control system can only reduce the vertical acceleration of the sprung mass in terms of roll and pitch, and reduces the vertical acceleration at each corner without considering driver and passenger locations and comfort.

Next, the driver and passengers' comfort will be considered in the control algorithm. This algorithm considers that the total center of gravity of the driver and passengers varies as the number of people in the vehicle may vary.

The derivation is following the way to derive HCC [23] and this modified HCC control system is based on the vertical acceleration of passengers, not on the force or momentum of the vehicle itself.

Since the capacity of regular vehicle is normally 4 passengers (2 in front and 2 in back) only four passengers are considered in this case. Note that the number of passengers in the algorithm can change according to the capacity of the vehicle. The vector a_{pz} which is a matrix of the vertical acceleration of each passenger has taken each passenger into account so that it is possible to change the passenger which will be weighted more or less in this control algorithm.

In the case when only the driver is in the vehicle, the total center of gravity will be leaned to the driver at all times so that it is possible to improve the driver's comfort by reducing the vertical acceleration of the total center of gravity. Furthermore, since the center of gravity of the driver is also

affected by the roll and pitch acceleration of the sprung mass and the suspension systems, the vertical acceleration of the driver based on the full car model in Figure 3 in SAE coordinate system is [9]:

$$a_{pz} = \begin{Bmatrix} a_{pz1}\,(Front\ Left\ Seat) \\ a_{pz2}\,(Front\ Right\ Seat) \\ a_{pz3}\,(Rear\ Left\ Seat) \\ a_{pz4}\,(Rear\ Right\ Seat) \end{Bmatrix} = \begin{Bmatrix} a_{CG} - L_8\ddot{\phi} - L_3\ddot{\theta} \\ a_{CG} + L_7\ddot{\phi} - L_3\ddot{\theta} \\ a_{CG} - L_8\ddot{\phi} + L_4\ddot{\theta} \\ a_{CG} + L_7\ddot{\phi} + L_4\ddot{\theta} \end{Bmatrix} \quad (4.7)$$

where

$$\begin{aligned} \ddot{\theta} = \Big\{ & \big(L_1(k_{s1}+k_{s2}) - L_2(k_{s3}+k_{s4})\big)z + \big(L_1(c_{s1}+c_{s2}) - L_2(c_{s3}+c_{s4})\big)\dot{z} \\ & + \Big(L_1^2(k_{s1}+k_{s2}) - L_2^2(k_{s3}+k_{s4})\Big)\theta \\ & + \Big(L_1^2(c_{s1}+c_{s2}) - L_2^2(c_{s3}+c_{s4})\Big)\dot{\theta} + L_1k_{s1}x_{u1} + L_1c_{s1}\dot{x}_{u1} \\ & + L_1k_{s2}x_{u2} + L_1c_{s2}\dot{x}_{u2} - L_2k_{s3}x_{u3} - L_2c_{s3}\dot{x}_{u3} - L_2k_{s4}x_{u4} \\ & - L_2c_{s4}\dot{x}_{u4} + L_1f_{z1} + L_1f_{z2} - L_2f_{z3} - L_2f_{z4}\Big\}/I_{yy} \end{aligned} \quad (4.8)$$

$$\begin{aligned} \ddot{\phi} = \Big\{ & -\left(\frac{L_5+L_6}{2}\right)^2 (k_{s1}+k_{s2}+k_{s3}+k_{s4})\phi \\ & - \left(\frac{L_5+L_6}{2}\right)^2 (c_{s1}+c_{s2}+c_{s3}+c_{s4})\dot{\phi} \\ & + \frac{L_5+L_6}{2}(k_{s1}x_{u1} + c_{s1}\dot{x}_{u1} - k_{s2}x_{u2} - c_{s2}\dot{x}_{u2} + k_{s3}x_{u3} \\ & + c_{s3}\dot{x}_{u3} - k_{s4}x_{u4} - c_{s4}\dot{x}_{u4} + f_{z1} - f_{z2} + f_{z3} - f_{z4})\Big\}/I_{xx} \end{aligned} \quad (4.9)$$

Note that there are damping forces at each corner in Equation (4. 8) and Equation (4. 9).

For the Jacobian matrix,

$$Jac_{4\times4} = \begin{bmatrix} \frac{\partial a_{pz1}}{\partial f_{z1}} & \frac{\partial a_{pz1}}{\partial f_{z2}} & \frac{\partial a_{pz1}}{\partial f_{z3}} & \frac{\partial a_{pz1}}{\partial f_{z4}} \\ \frac{\partial a_{pz2}}{\partial f_{z1}} & \frac{\partial a_{pz2}}{\partial f_{z2}} & \frac{\partial a_{pz2}}{\partial f_{z3}} & \frac{\partial a_{pz2}}{\partial f_{z4}} \\ \frac{\partial a_{pz3}}{\partial f_{z1}} & \frac{\partial a_{pz3}}{\partial f_{z2}} & \frac{\partial a_{pz3}}{\partial f_{z3}} & \frac{\partial a_{pz3}}{\partial f_{z4}} \\ \frac{\partial a_{pz4}}{\partial f_{z1}} & \frac{\partial a_{pz4}}{\partial f_{z2}} & \frac{\partial a_{pz4}}{\partial f_{z3}} & \frac{\partial a_{pz4}}{\partial f_{z4}} \end{bmatrix} \quad (4.10)$$

where

$$\frac{\partial a_{pz1}}{\partial f_{z1}} = \frac{1}{m_s} - L_8\left(\frac{L_5 + L_6}{2I_{xx}}\right) - L_3\left(\frac{L_1}{I_{yy}}\right) \quad \textbf{(4. 11)}$$

$$\frac{\partial a_{pz1}}{\partial f_{z2}} = \frac{1}{m_s} + L_8\left(\frac{L_5 + L_6}{2I_{xx}}\right) - L_3\left(\frac{L_1}{I_{yy}}\right) \quad \textbf{(4. 12)}$$

$$\frac{\partial a_{pz1}}{\partial f_{z3}} = \frac{1}{m_s} - L_8\left(\frac{L_5 + L_6}{2I_{xx}}\right) + L_3\left(\frac{L_2}{I_{yy}}\right) \quad \textbf{(4. 13)}$$

$$\frac{\partial a_{pz1}}{\partial f_{z4}} = \frac{1}{m_s} + L_8\left(\frac{L_5 + L_6}{2I_{xx}}\right) + L_3\left(\frac{L_2}{I_{yy}}\right) \quad \textbf{(4. 14)}$$

$$\frac{\partial a_{pz2}}{\partial f_{z1}} = \frac{1}{m_s} + L_7\left(\frac{L_5 + L_6}{2I_{xx}}\right) - L_3\left(\frac{L_1}{I_{yy}}\right) \quad \textbf{(4. 15)}$$

$$\frac{\partial a_{pz2}}{\partial f_{z2}} = \frac{1}{m_s} - L_7\left(\frac{L_5 + L_6}{2I_{xx}}\right) - L_3\left(\frac{L_1}{I_{yy}}\right) \quad \textbf{(4. 16)}$$

$$\frac{\partial a_{pz2}}{\partial f_{z3}} = \frac{1}{m_s} + L_7\left(\frac{L_5 + L_6}{2I_{xx}}\right) + L_3\left(\frac{L_2}{I_{yy}}\right) \quad \textbf{(4. 17)}$$

$$\frac{\partial a_{pz2}}{\partial f_{z4}} = \frac{1}{m_s} - L_7\left(\frac{L_5 + L_6}{2I_{xx}}\right) + L_3\left(\frac{L_2}{I_{yy}}\right) \quad \textbf{(4. 18)}$$

$$\frac{\partial a_{pz3}}{\partial f_{z1}} = \frac{1}{m_s} - L_8\left(\frac{L_5 + L_6}{2I_{xx}}\right) + L_4\left(\frac{L_1}{I_{yy}}\right) \quad \textbf{(4. 19)}$$

$$\frac{\partial a_{pz3}}{\partial f_{z2}} = \frac{1}{m_s} + L_8\left(\frac{L_5 + L_6}{2I_{xx}}\right) + L_4\left(\frac{L_1}{I_{yy}}\right) \quad \textbf{(4. 20)}$$

$$\frac{\partial a_{pz3}}{\partial f_{z3}} = \frac{1}{m_s} - L_8\left(\frac{L_5 + L_6}{2I_{xx}}\right) - L_4\left(\frac{L_2}{I_{yy}}\right) \quad \textbf{(4. 21)}$$

$$\frac{\partial a_{pz3}}{\partial f_{z4}} = \frac{1}{m_s} + L_8\left(\frac{L_5 + L_6}{2I_{xx}}\right) - L_4\left(\frac{L_2}{I_{yy}}\right) \quad \textbf{(4. 22)}$$

$$\frac{\partial a_{pz4}}{\partial f_{z1}} = \frac{1}{m_s} + L_7\left(\frac{L_5 + L_6}{2I_{xx}}\right) + L_4\left(\frac{L_1}{I_{yy}}\right) \quad \textbf{(4. 23)}$$

$$\frac{\partial a_{pz4}}{\partial f_{z2}} = \frac{1}{m_s} - L_7\left(\frac{L_5 + L_6}{2I_{xx}}\right) + L_4\left(\frac{L_1}{I_{yy}}\right) \quad \textbf{(4. 24)}$$

$$\frac{\partial a_{pz4}}{\partial f_{z3}} = \frac{1}{m_s} + L_7\left(\frac{L_5 + L_6}{2I_{xx}}\right) - L_4\left(\frac{L_2}{I_{yy}}\right) \quad \textbf{(4. 25)}$$

$$\frac{\partial a_{pz4}}{\partial f_{z4}} = \frac{1}{m_s} - L_7\left(\frac{L_5 + L_6}{2I_{xx}}\right) - L_4\left(\frac{L_2}{I_{yy}}\right) \quad \textbf{(4. 26)}$$

The error term in HCC objective function can be rewritten for this control algorithm as the following:

$$E = \left(a_{pzd} - a_{pz}\right) \tag{4.27}$$

where a_{pzd} is a desired value of the vertical acceleration, which is zero in this case, since the goal is to reduce the vertical acceleration as close to zero as possible for better ride comfort. In other words, the passengers should feel as less acceleration as possible for better ride comfort.

This vertical acceleration parameter can be written using the total and the adjustment of the vertical damping force at each corner, as follows:

$$a_{pz} = \Gamma(f_z + \delta f_z) \tag{4.28}$$

Therefore, the error tern in the objective function can be:

$$\begin{aligned} a_{pzd} - a_{pz} = a_{pzd} - \Gamma(f_z + \delta f_z) &= a_{pzd} - \left\{\Gamma(f_z) + \frac{\partial \Gamma}{\partial f_z}\delta f_z\right\} \\ &= \left\{a_{pzd} - \Gamma(f_z)\right\} - \frac{\partial \Gamma}{\partial f_z}\delta f_z \end{aligned} \tag{4.29}$$

3.3 Force Distribution (Allocation) Using the Weighting Matrix

The advantage of this control algorithm is that it is possible to turn on and off the controller for some passenger seat locations, so that the controller can focus on a specific passenger seat location. W_E in the objective function is the four by four weighting matrix, as follows:

$$W_E = \begin{bmatrix} W_{E(a_{pz1})} & 0 & 0 & 0 \\ 0 & W_{E(a_{pz2})} & 0 & 0 \\ 0 & 0 & W_{E(a_{pz3})} & 0 \\ 0 & 0 & 0 & W_{E(a_{pz4})} \end{bmatrix} \tag{4.30}$$

It is possible to weight any of these four elements for any passenger seat location by defining the elements 0 or 1.

For instance, if a baby sits on the rear-right passenger seat location, and the requirement is to improve ride comfort only for that location, it is possible to set $W_{E(a_{pz1})}$, $W_{E(a_{pz2})}$, and $W_{E(a_{pz3})}$ to zero and $W_{E(a_{pz4})}$ to 1, then the localized-based controller will only focus on the location where the baby is sitting to reduce the vertical vibration and provide better ride comfort.

Alternatively, if there is only one driver in a vehicle, it is also possible to turn off the weighting elements for other seat locations, except the front-left passenger seat location of the driver. Then, the localized-based controller improves ride comfort only at the specific seat location for the driver.

The localized-based controller is expected to save energy, since the suspension system of the vehicle does not have to generate the required energy to reduce the vertical acceleration at every seat location. By limiting the controller focus to a specific seat location, the suspension system only needs to provide the necessary, but not redundant force that the controller asks.

In this research, QCAT (Quadratic Programming Control Allocation Toolbox) is used to find the optimal solution within the range of the available damping force [24].

3.4 Results

Firstly, the vertical acceleration at the front-left passenger seat location is shown in Figure 22. When the vehicle's front wheels hit the bump, the passive suspension system shows better response than other systems because the localized-based control algorithm uses the distances between the center of gravity and each passenger seat locations to control the vertical acceleration at each location. Particularly for the front seat locations, the effect of minimizing the pitch and roll acceleration is relatively weaker than that for the rear seat locations, since the front seat locations are closer to the center of gravity of the vehicle model than to the rear seat locations. As a result, the impacts on the front seat locations using the localized-based controller are expected to be minimal compared to other locations.

When the rear wheels hit the bump, even though the localized-based controller with the semi-active suspension system has several higher peak values at the beginning, the controller shows faster stabilizing time than the passive suspension system.

As in Table 7, the localized-based controller with the semi-active and active suspension systems improves ride comfort more than the passive suspension system.

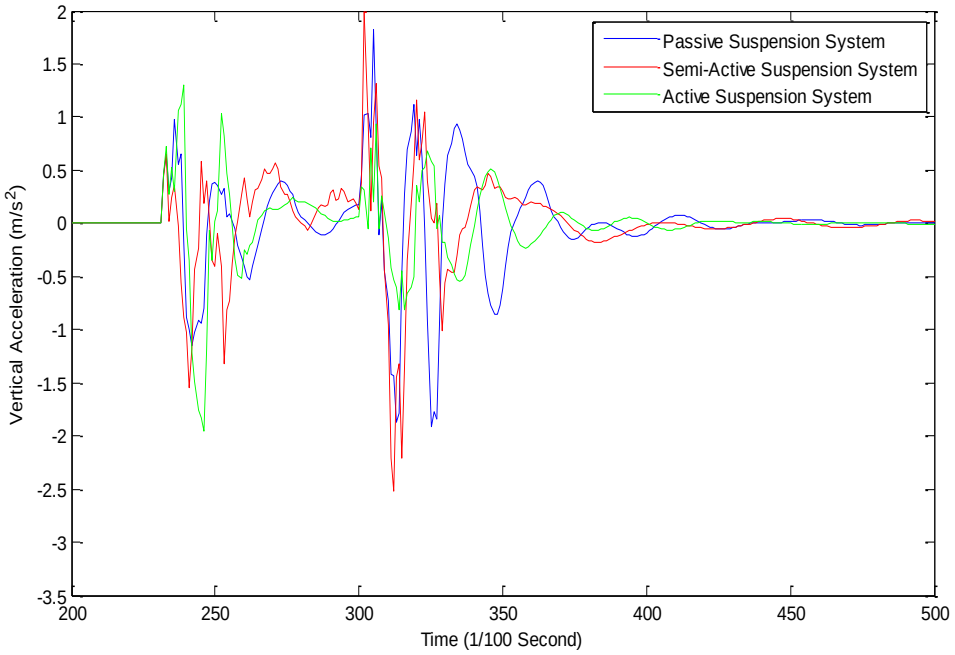

Figure 22: Vertical Acceleration at the Front Left Passenger Seat Location with Localized-Based Control Algorithm (Different Suspension Systems)

Table 7: RMS of the Vertical Acceleration at the Front Left Passenger Seat Location with Localized-Based Control Algorithm (Different Suspension Systems)

	RMS	Difference (Relative to Passive)
Passive	0.2413	0 %
Localized-Based controller (Semi-Active)	0.2337	3.15 %
Localized-Based controller (Active)	0.1873	22.38 %

Second, the vertical acceleration at the rear-left passenger seat location is depicted in Figure 23. Similar to the front-left passenger seat location, the vertical acceleration at the rear-left passenger seat location is reduced by using the localized-based controller.

According to RMS values depicted in Table 8, it is seen that the vertical acceleration at the rear-left passenger seat location experiences a greater reduction than the front-left passenger seat location with the localized-based control algorithm. This is a result of the characteristics of the localized-based controller, as mentioned earlier.

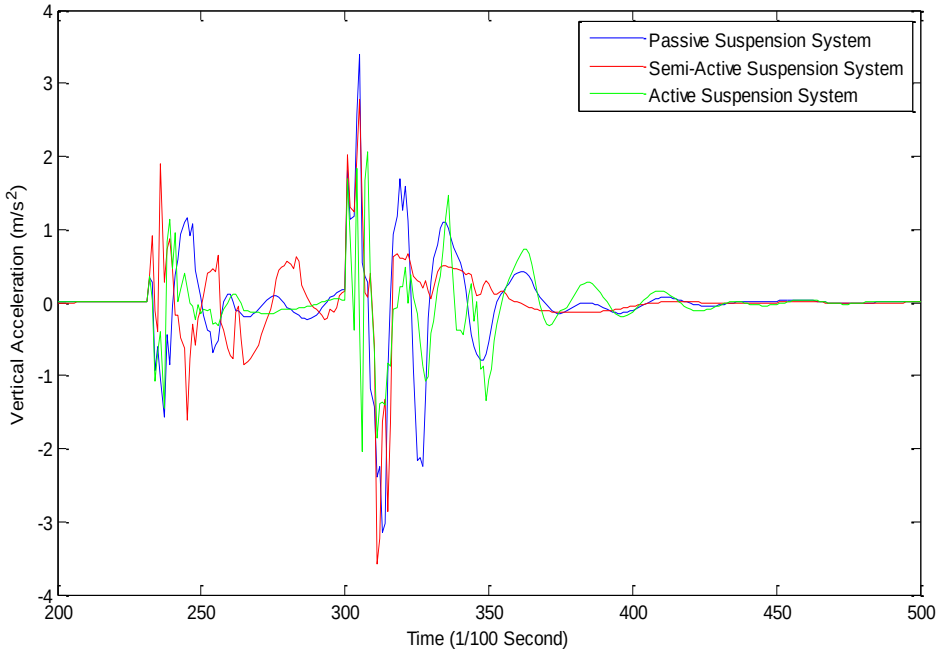

Figure 23: Vertical Acceleration at the Rear Left Passenger Seat Location with Localized-Based Control Algorithm (Different Suspension Systems)

Table 8: RMS of the Vertical Acceleration at the Rear Left Passenger Seat Location with Localized-Based Control Algorithm (Different Suspension Systems)

	RMS	Difference (Relative to Passive)
Passive	0.3365	0 %
Localized-Based controller (Semi-Active)	0.2939	12.66 %
Localized-Based controller (Active)	0.2401	28.65 %

Last, the vertical acceleration at the further location, which is located 1 meter behind the rear-left passenger seat, is shown in Figure 24. Overall, the localized-based controller with the semi-active and

the active suspension systems reduce the vertical acceleration at this location in terms of a peak value and oscillation.

Furthermore, the effect of the controller on the vertical acceleration at this location is larger than the previous two locations. It is likely that Localized-Base control algorithm can reduce the vertical acceleration more at a further location from the center of gravity. This also means that this controller can provide better ride comfort if it is applied to some longitudinally extended vehicle, such as a limousine, or a conventional vehicle.

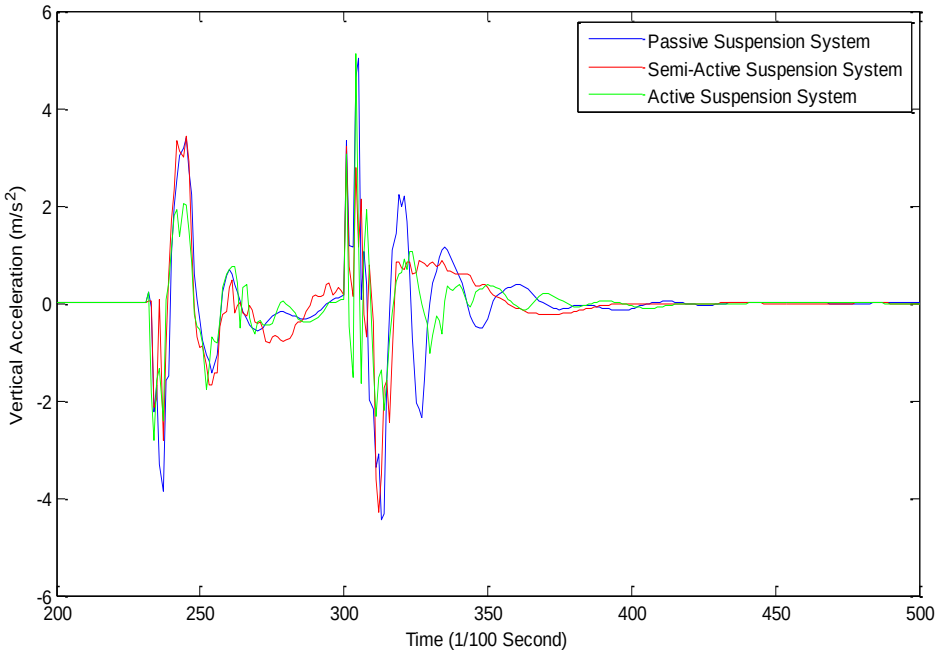

Figure 24: Vertical Acceleration at the Further Location with Localized-Based Control Algorithm (Different Suspension Systems)

Table 9: RMS of the Vertical Acceleration at the Further Location with Localized-Based Control Algorithm (Different Suspension Systems)

	RMS	Difference (Relative to Passive)
Passive	0.5361	0 %
Localized-Based controller (Semi-Active)	0.4451	16.97 %
Localized-Based controller (Active)	0.3646	31.99 %

Figure 25 shows the vertical acceleration at the front-left passenger seat location with the passive suspension system, the skyhook, and the localized-based controller with the semi-active suspension system to compare them with the semi-active suspension system, since the actual vehicle model, Cadillac STS, uses the semi-active suspension system.

The skyhook and localized-based controllers do not seem to reduce the high peaks when the front and rear wheels hit the bump respectively. However, they significantly prevent oscillation after the rear wheels hit the bump.

As shown in Table 10, both the skyhook and localized-based controllers reduce the RMS values of the vertical acceleration with the semi-active suspension system. The effects, however, are minimal on this location.

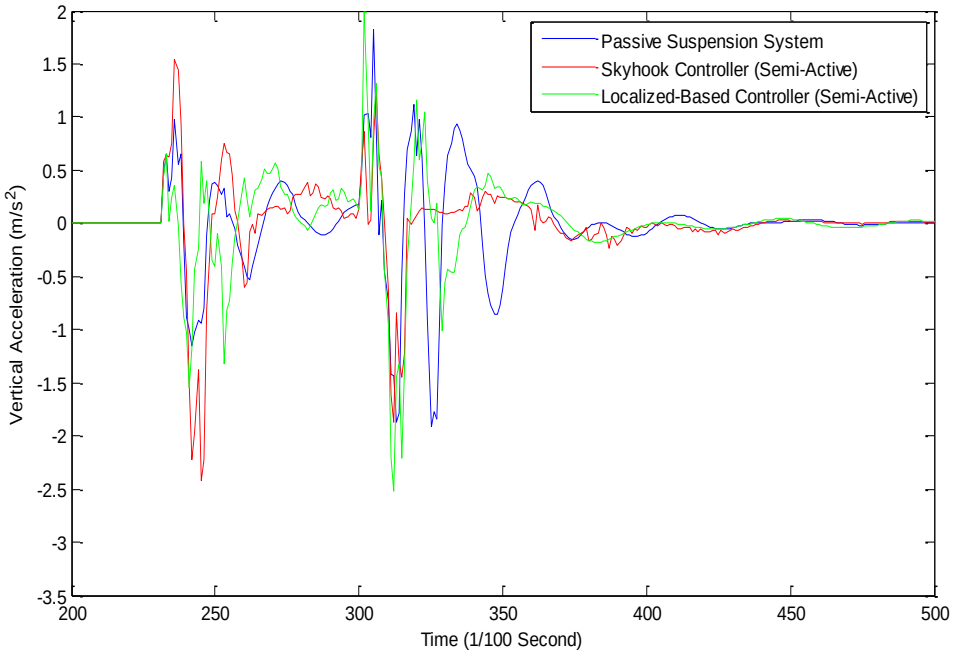

Figure 25: Vertical Acceleration at the Front Left Passenger Seat Location with Different Control Algorithm (Semi-Active Suspension System)

Table 10: RMS of the Vertical Acceleration at the Front Left Passenger Seat Location with Different Control Algorithm (Semi-Active Suspension System)

	RMS	Difference (Relative to Passive)
Passive	0.2413	0 %
Skyhook controller (Semi-Active)	0.2338	3.10 %
Localized-Based controller (Semi-Active)	0.2337	3.15 %

Figure 26 shows the vertical accelerations at the rear-left passenger seat location with different controllers. Overall, the effect of the skyhook and localized-based controllers with the semi-active suspension system is bigger than that at the front-left passenger seat location due to the characteristics of the localized-based control algorithm and the distance between the center of gravity and the seat location.

RMS values of the vertical acceleration at this location are also shown in Table 11. As shown, the localized-based controller improves RMS value more than the skyhook does. In addition, the impact of the controllers at this location is bigger than that at the front-left passenger seat location as well.

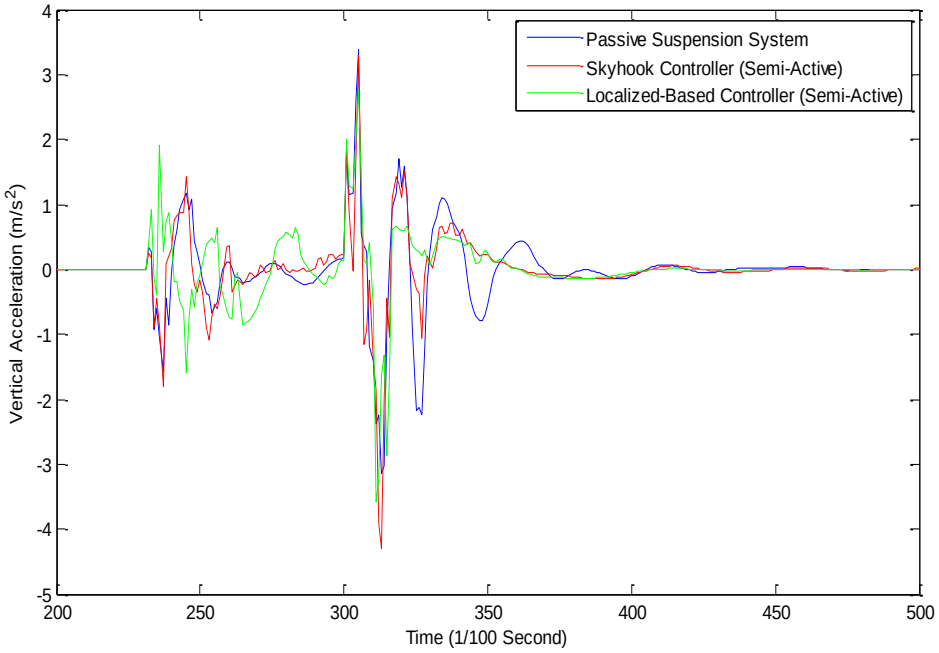

Figure 26: Vertical Acceleration at the Rear Left Passenger Seat Location with Different Control Algorithm (Semi-Active Suspension System)

Table 11: RMS of the Vertical Acceleration at the Rear Left Passenger Seat Location with Different Control Algorithm (Semi-Active Suspension System)

	RMS	Difference (Relative to Passive)
Passive	0.3365	0 %
Skyhook controller (Semi-Active)	0.3130	6.98 %
Localized-Based controller (Semi-Active)	0.2939	12.66 %

Last, Figure 27 depicts the vertical accelerations at the further location with controllers. Generally, the controllers with a semi-active suspension system show better performance than the passive suspension system. The peak values of the vertical accelerations are reduced significantly by 30%

when the rear wheels hit the bump. Furthermore, after the vehicle model passes the bump, the controllers stabilize the vehicle model faster than the passive suspension system.

Table 12 depicts RMS values of the vertical acceleration at this location. The skyhook controller improves ride comfort based on RMS value, but the localized-based controller provides better ride comfort than the skyhook controller.

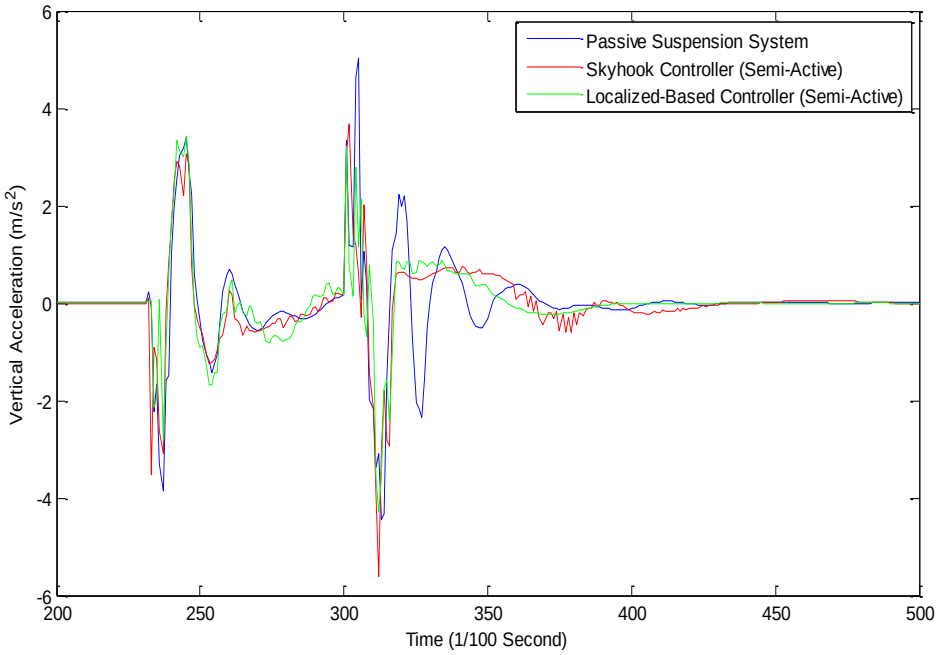

Figure 27: Vertical Acceleration at the Further Location with Different Control Algorithm (Semi-Active Suspension System)

Table 12: RMS of the Vertical Acceleration at the Further Location with Different Control Algorithm (Semi-Active Suspension System)

	RMS	Difference (Relative to Passive)
Passive	0.5361	0 %
Skyhook controller (Semi-Active)	0.4756	11.29 %
Localized-Based controller (Semi-Active)	0.4451	16.97 %

The localized-based controller with the semi-active suspension system is also tested on the type-B random road profile to compare it to the passive suspension system. Table 13 shows RMS values of the vertical accelerations at the different passenger seat locations and the percentage difference between the passive suspension system and localized-based controller with the semi-active suspension system.

As depicted, the localized-based controller reduces the overall vertical accelerations at all locations. RMS at the rear-left passenger sear location, however, has less improvement than that at the front-left passenger seat location. It is assumed that since the random road profile is very high frequency the localized-based controller has a limited ability to reduce the vertical acceleration of the sprung mass using the semi-active suspension system.

Table 13: RMS of the Vertical Acceleration at Different Passenger Seat Locations with Localized-Based Control Algorithm and Semi-Active Suspension System on Random Road

	RMS		Difference
	Passive	Localized-Based	
Front Left	0.4872	0.4608	5.42 %
Rear Left	0.6539	0.6312	3.47 %
Further	1.0324	0.9023	12.60 %

In sum, Localized-Base controller reduces the RMS values of the vertical accelerations at any locations on the vehicle model more than the passive and skyhook controller. Even though the localized-based controller cannot reduce the peak values significantly, it is promising that the controller can provide better ride comfort to passengers in terms of RMS values.

In addition, unlike the ordinary control algorithm for ride comfort, it is convenient to adjust the localized-based controller for any other vehicle model by changing the physical properties, such as the distances between the center of gravity and passenger seat locations, and physical length of a vehicle model.

Chapter 4
Experimental Studies

4.1 Implementation of Control Algorithms on Test Vehicle

The performance of the algorithms discussed in the previous chapters has been evaluated experimentally on a Cadillac STS. Figure 28 features a diagram of the whole system as set for the test.

Two different sensors attached to the vehicle collect data regarding vehicle motion. One is a six-axis inertial navigation system (OXTS-RT2500, Datron technology) which measures the linear acceleration and velocity of the vehicle along all three axes, longitudinal, lateral and vertical, as well as three angular rates along the axes based on SAE coordinate system [19] [25] [26]. The collected values of only pitch and roll rates, and also the vertical acceleration of the vehicle will be used for the controller. The second sensor is a height sensor located at each corner of the vehicle, where it is close enough to each wheel to measure the distance from the ground for the controller [27].

The data for these sensors goes to a dSpace Autobox [28], which is mounted inside the vehicle trunk. The control algorithm is stored in Autobox and Autobox receives the data from the sensors and generates the output required to control the vehicle. However, the output from Autobox is not the current; rather it is the PWM (Pulse-Width Modulation) signal.

PWM signal goes to the current driver (AZ20A8DDC from Advanced Motion Controls) which generates the current bases on PWM signal's duty cycle. On the same circuit board, there are four current drivers and each of them is responsible for the MR damper at each corner [29].

Last, the current signal goes to the MR damper of each suspension system. Regarding the current signal, the viscosity of the fluid in the damper will change to reduce the vertical motion at each corner.

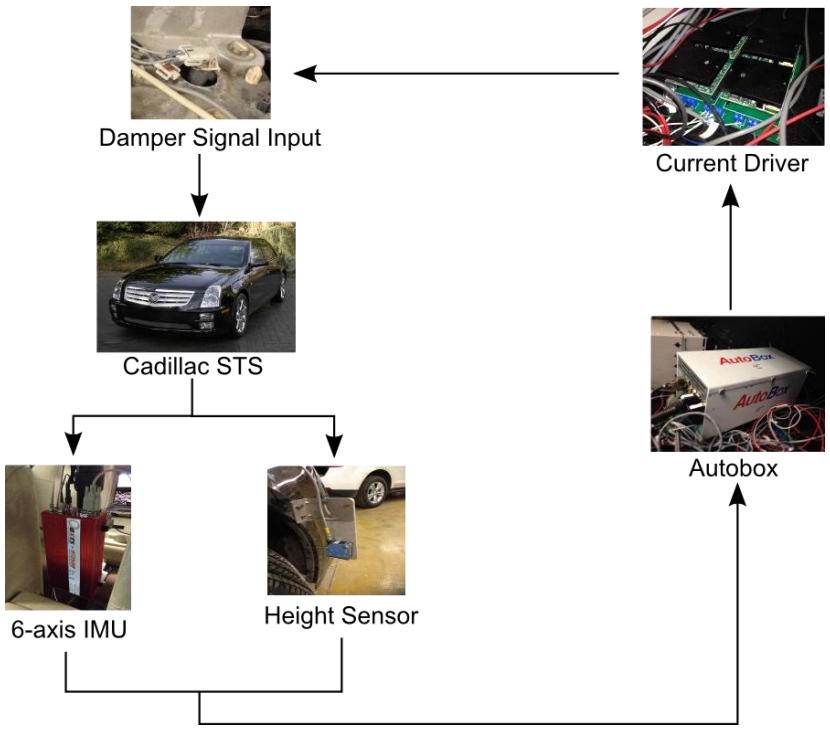

Figure 28: Diagram of Hardware-In-The-Loop System

4.2 Characterization of MR Damper

Before utilizing the existing damping characteristics of the suspension system of Cadillac STS, studied by Ankur Agrawal [19], another test for the damping characteristics is executed with the same method used by Agrawal in [19].

In order to obtain the damping characteristics, the damper is tested with different constant current inputs of 0, 0.5, 1, 1.5, 2.0, 2.5, 3.0, 3.5, and 4.0 A. Among these currents, the test results of the damping characteristics at $i = 1.5$A and $i = 3.5$A of the front and rear-left dampers are depicted in Figure 29, Figure 30, Figure 31, and Figure 32 respectively.

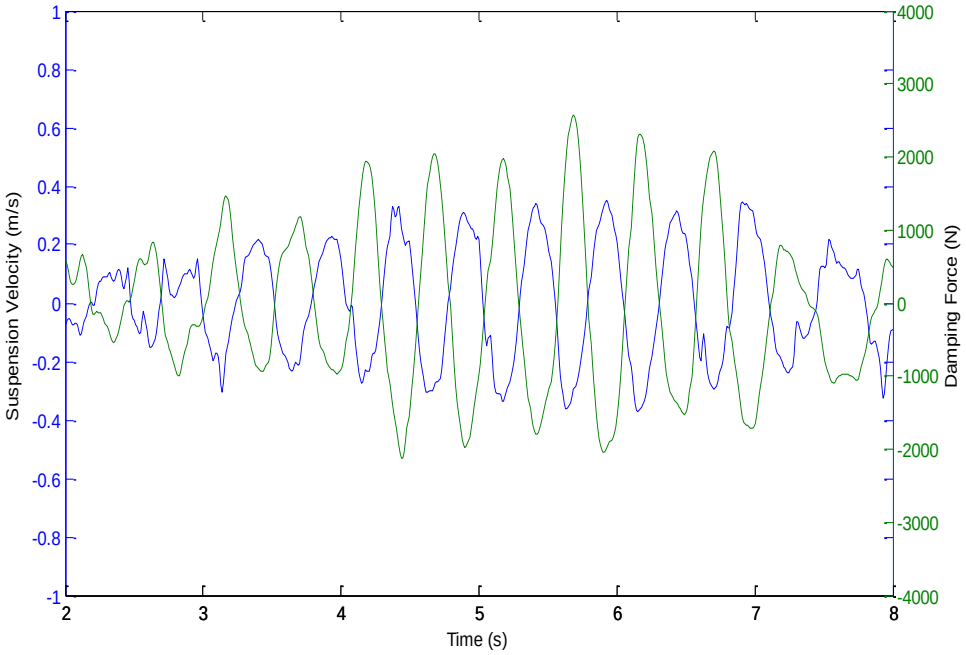

Figure 29: Damping Characteristic at *i* = 1A of the Front Left Damper

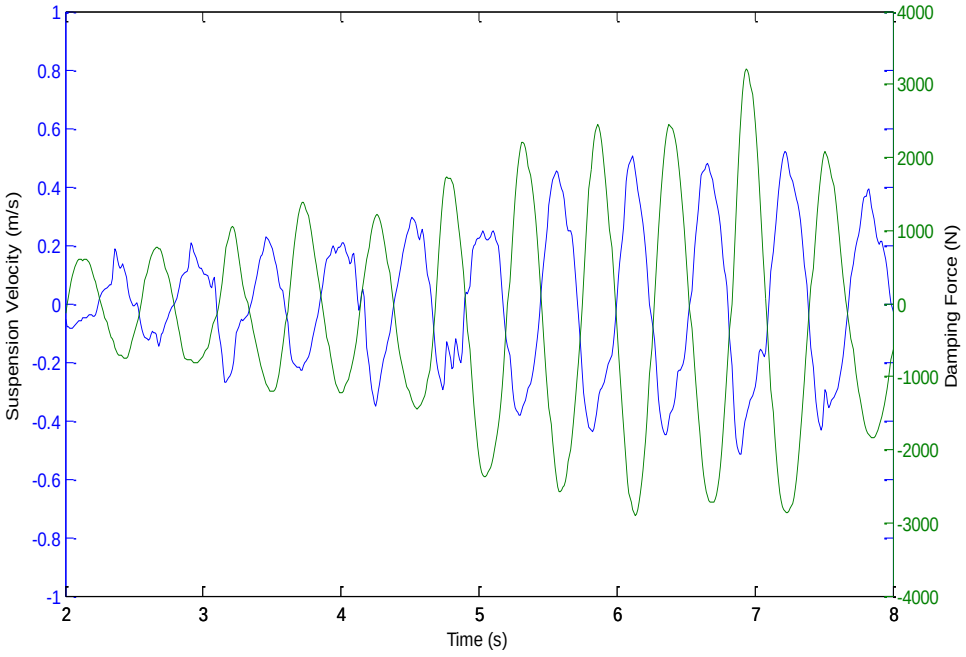

Figure 30: Damping Characteristic at *i* = 3A of the Front Left Damper

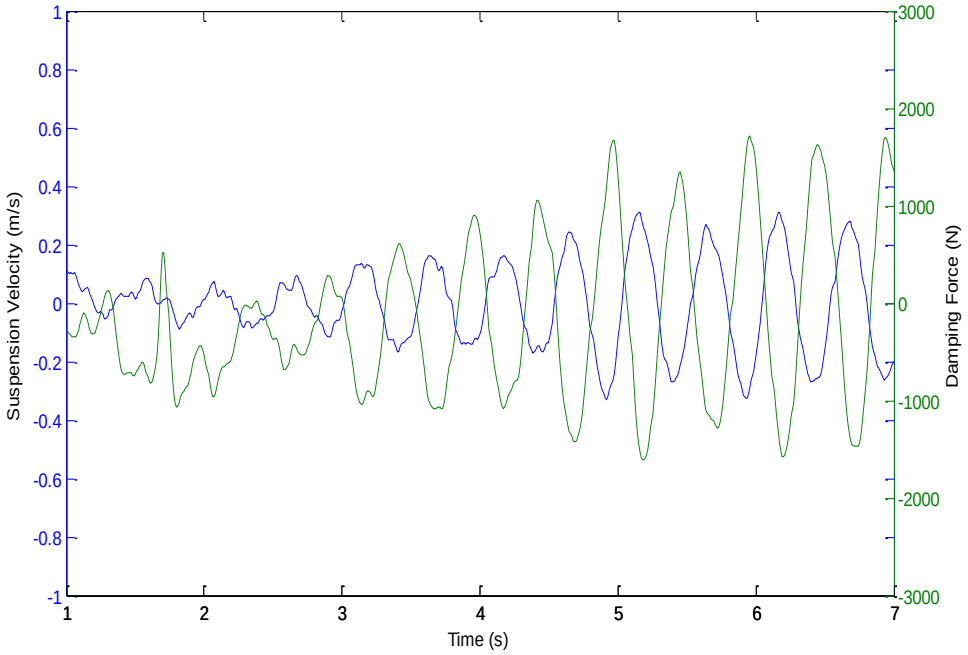

Figure 31: Damping Characteristic at *i* = 1A of the Rear Left Damper

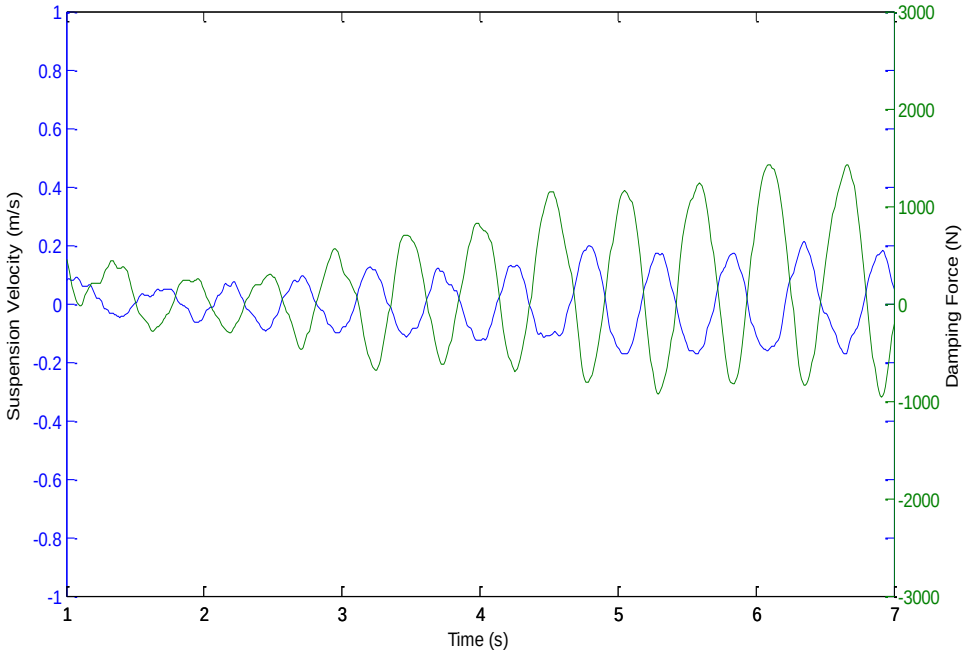

Figure 32: Damping Characteristic at *i* = 3A of the Rear Left Damper

By using the data of the damping characteristics from the test, data for mapping damping characteristics can be prepared. As shown in Figure 33 and Figure 34, the damping characteristics of the front and the rear-left suspensions in 3D map are different from each other since Cadillac STS uses different suspension systems on the front and the rear axles. However, the left and the right suspensions on the same axle are the same, so it is possible to use the same damping characteristics for the both sides of the same axle.

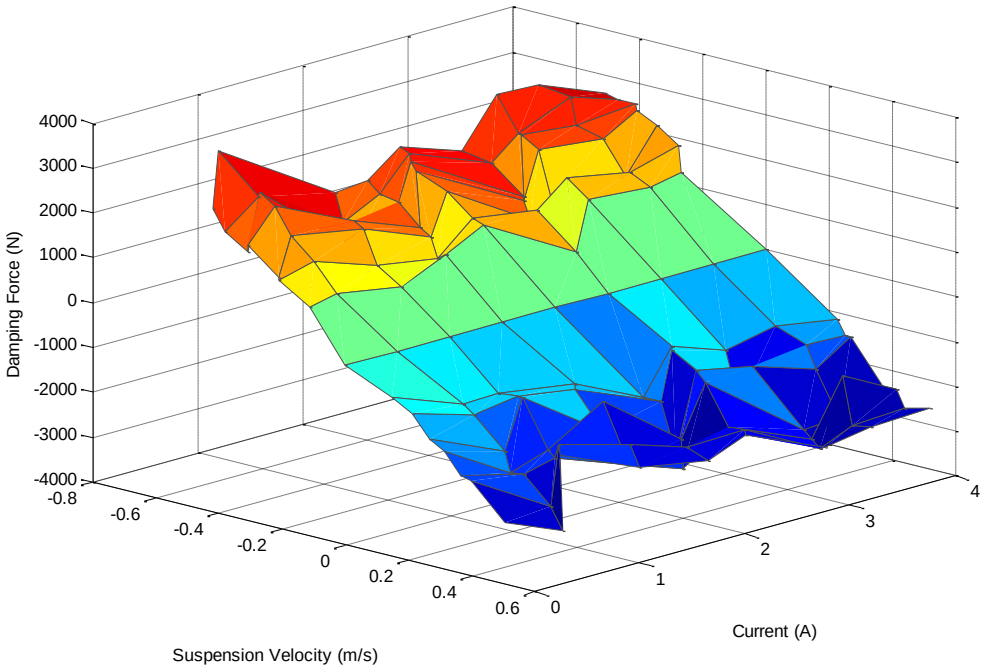

Figure 33: Damping Characteristics of the Front Left Suspension

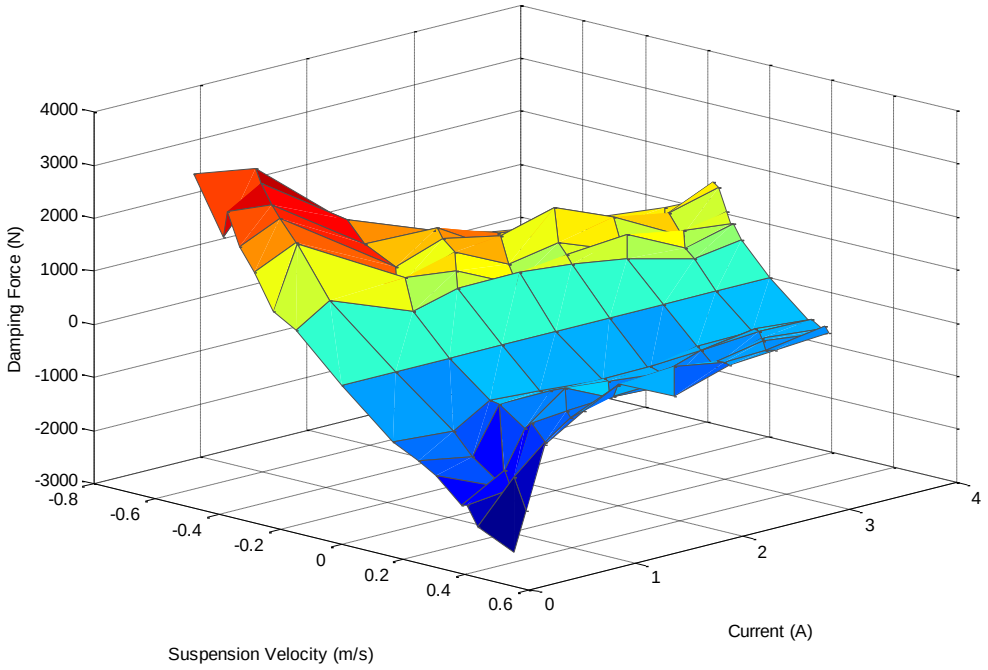

Figure 34: Damping Characteristics of the Rear Left Suspension

According to the obtained damping characteristics from the test, both of the damping characteristics of the front and the rear suspension systems seem to be linear, so they can be expressed as a linear equation rather than using a look-up table in the control algorithm for a faster response. In addition, the suspension velocity maintaining a range from -0.6 m/s to 0.5 m/s is visible. Compared to Agrawal's damping characteristics, the range of the suspension velocity is narrower than that of Agrawal's. However, since the harsh pitching maneuver is performed during the test, it is not expected that the suspension velocity exceeds the range when the test for ride comfort is executed. Therefore, theses damping characteristics are also feasible with the control algorithm.

For mapping, the polynomial curve fitting with the collected data points is used to obtain the linear equations. The linear equations for the front and rear dampers are expressed as:

$$f_d = \begin{cases} (-25.4118 \times i - 5655.4022) \times v & \text{for the front left damper} \\ (-474.5705 \times i - 5361.0407) \times v & \text{for the rear left damper} \end{cases} \quad \textbf{(5.1)}$$

where i and v are the current and the suspension velocity respectively.

For the inverse-mapping, linear equations for the current, i, are obtained by rearranging Equation (5. 1) for i as follows:

$$i = \begin{cases} -(f_d/v + 5655.4022)/25.4118 & \text{for the front left damper} \\ -(f_d/v + 5361.0407)/474.5705 & \text{for the rear left damper} \end{cases} \quad \textbf{(5. 2)}$$

where f_d and v are the damping force and the suspension velocity respectively.

Note that the damping characteristics obtained from the experiment have less difference of its slope with respect to the current, i. According to Agrawal's damping characteristics in Figure 12, they have steeper slopes with respect to the increasing i even within the same range as the obtained one. In addition, both the obtained damping characteristics of the front and rear-left suspension systems have similarities regarding the amount of the damping force generated based on the suspension velocity.

Using the new control algorithm with Agrawal's and the obtained damping characteristics, multiple test drives are performed to compare vertical accelerations at different passenger seat locations. Figure 35, Figure 36, and **37** show the vertical accelerations at the front-left, rear-left, and farther passenger seat location when different damping characteristics are applied, respectively.

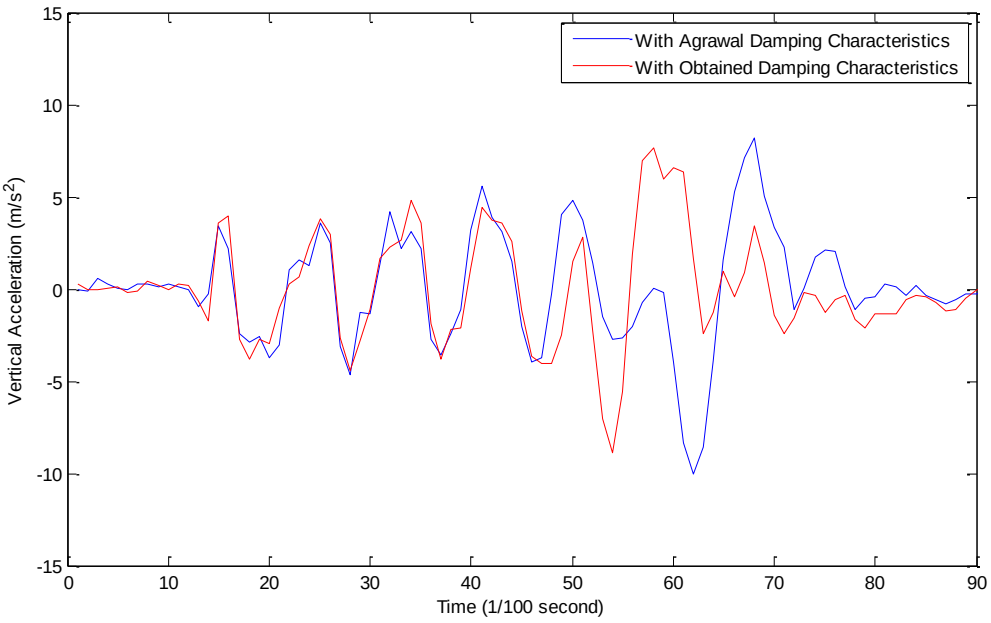

Figure 35: Vertical Acceleration at the Front Left Passenger Seat Location with Different Damping Characteristics

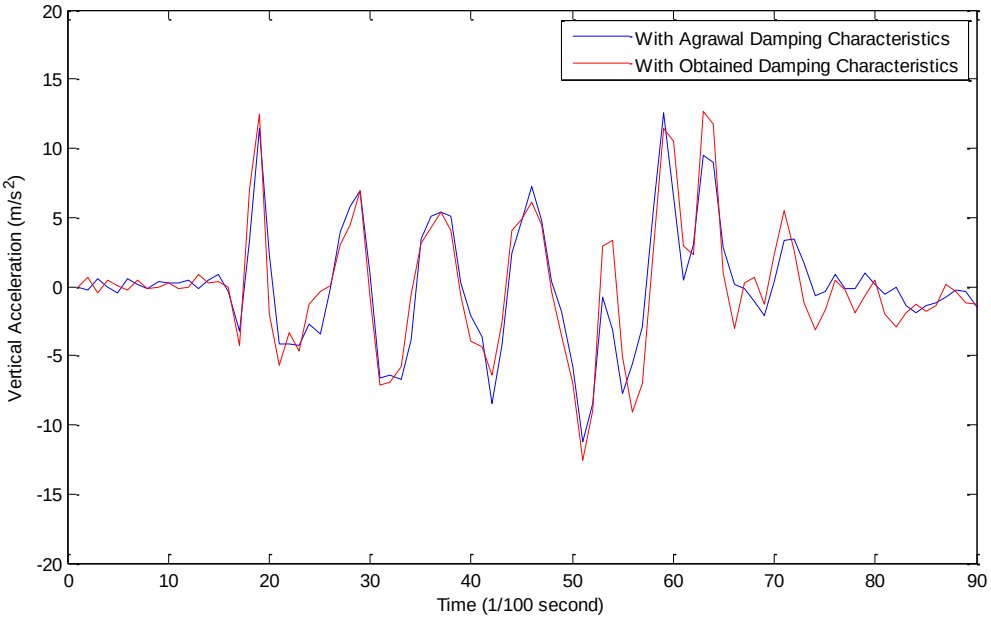

Figure 36: Vertical Acceleration at the Rear Left Passenger Seat Location with Different Damping Characteristics

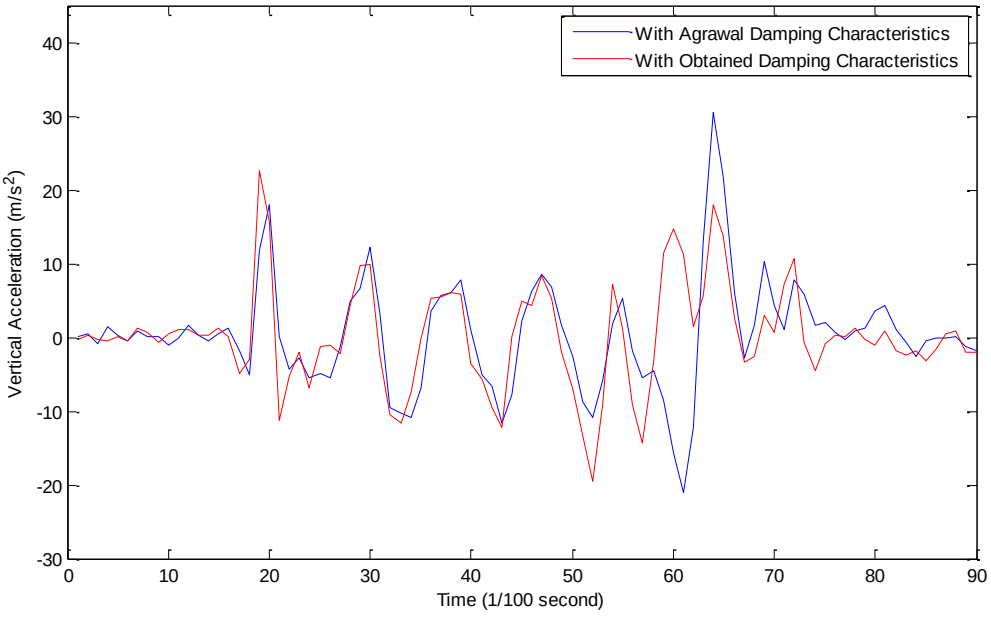

Figure 37: Vertical Acceleration at the Rear Left Passenger Seat Location with Different Damping Characteristics

The responses of the sprung mass seem to be similar to each other at the same passenger seat location. Therefore, it can be assumed that both of Agrawal's and the obtained damping characteristics can be used for the test drive. For the test drive, Agrawal's damping is adopted to work with the control algorithms, since Agrawal's model includes a wider range of the suspension velocity and distinct slopes of the curves at different currents.

4.3 Results

For the experiment, a single bump on the straight lane is tested using the Cadillac STS vehicle. The shape and the specification of the bump are shown in Figure 15 and Table 1 respectively.

Firstly, the Cadillac was driven in a straight direction at a constant speed of 30 kph to hit a single bump. The bump hits the vehicle's front tires and the rear tires at the same time respectively.

For the testing, several conditions are applied to the vehicle's suspension system in order to compare the new control algorithm with the conventional passive suspension system and the widely-used traditional skyhook control algorithm. Since the vehicle is equipped with the semi-active suspension system, it is possible to change the current applied directly to its damper by setting the variables of the current in dSpace. Therefore, in order to make the suspension system passive, the variables are set as constant values.

Other variables such as passengers' weights and road condition are also controlled to be constant as well to obtain a fair comparison.

Since the localized-based controller can be made to focus on any location on the vehicle by changing the weighting matrix, the front-left passenger seat, the driver seat, is taken as a reference point to compare the new controller with the passive suspension system and skyhook controller. Figure 38 shows the vertical accelerations of the chosen location, which is the front-left passenger seat location, with the three different control algorithms.

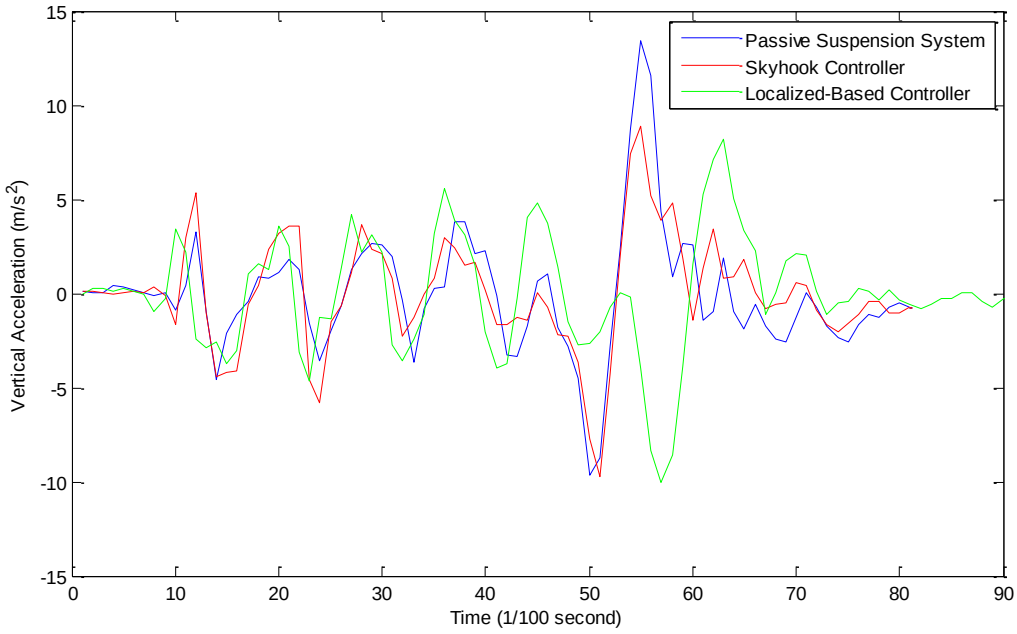

Figure 38: Vertical Acceleration at the Front Left Passenger Seat with Different Control Algorithms from the Test Drive

As shown in Figure 38, it can be seen that the maximum peak is reduced when using the skyhook and localized-based controllers. Since the seat location is close to the center of gravity, these control algorithms do not seem to have a significant effect on the vertical acceleration at the seat location.

The RMS of the vertical acceleration in each case is calculated as follows:

Table 14: RMS of Vertical Acceleration at the Front Left Passenger Seat with Different Control Algorithms from the Test Drive

	RMS	Difference (Relative to Passive)
Passive	3.0703	0 %
Skyhook	2.8280	7.89 %
Localized-based	3.0504	0.65 %

In terms of RMS, it is seen that the skyhook controller affected the vertical acceleration more than the localized-based controller. In other words, ride comfort of a passenger is better by using the skyhook control algorithm. Like the simulations shown in Chapter 3, this result is predicted due to the

limitation of the characteristic of the localized-based control algorithm. As mentioned in Chapter 3, the length between the center of gravity and the front-left passenger seat location in the localized-based control algorithm plays a significant role to minimize the vertical acceleration at the passenger seat location. This is because it is predicted that the closer to the center of gravity that a passenger seat location is, the smaller the effect of the localized-based controller is.

To ensure the localized-based controller works on other passenger seat locations, several other locations are tested to compare the vertical accelerations of the seat locations with those of the front-left passenger seat location.

Figure 39 shows vertical accelerations of the rear-left passenger seat location with the passive suspension system, skyhook, and localized-based controllers.

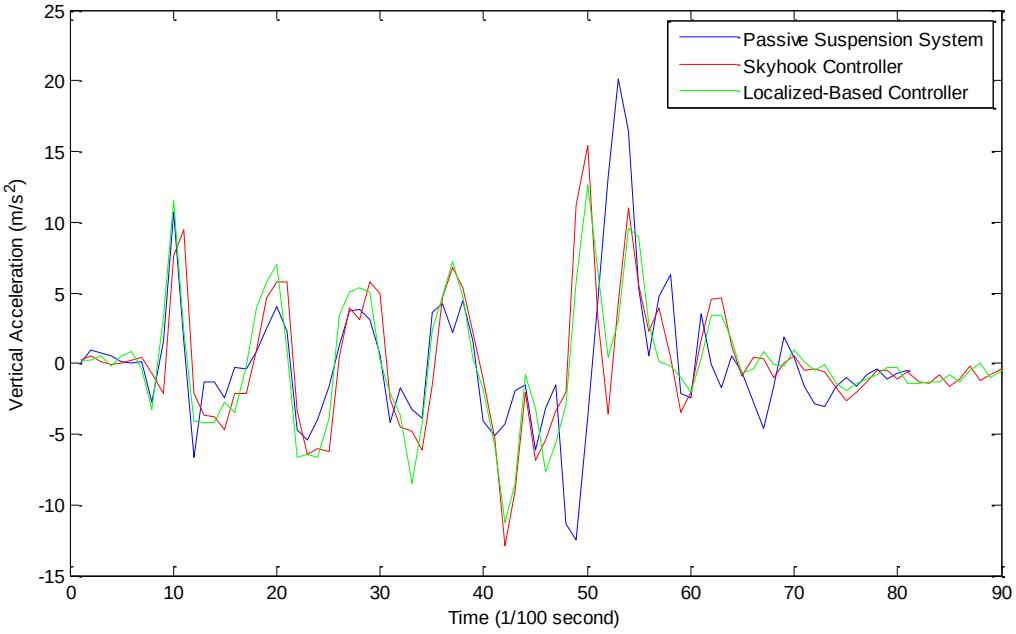

Figure 39: Vertical Acceleration at the Rear Left Passenger Seat Location with Different Control Algorithms from the Test Drive

As shown in Figure 39, the maximum peak is reduced when using the skyhook and localized-based controllers in the period of time between 40/100 to 60/100 seconds. Table 15 shows the RMS of the vertical accelerations at the rear-left passenger seat location.

Table 15: RMS of Vertical Acceleration at the Rear Left Passenger Seat Location with Different Control Algorithms from the Test Drive

	RMS	Difference (Relative to Passive)
Passive	4.5594	0 %
Skyhook	4.3872	3.78 %
Localized-Based	4.1904	8.09 %

It should be considered that both the skyhook and localized-based controllers have effects on the passenger's vertical acceleration, ride comfort, in terms of the RMS values in Table 15. Specifically, the localized-based controller is showing better performance than the skyhook controller. Even though those RMS values are not similar to the simulations in Chapter 3, it can be said that the controllers are affecting passenger's ride comfort in the way that was expected.

The further location, which is 1 meter behind the rear-left passenger seat location, is taken into account after the experiment for the rear-left passenger seat location. The reason why this location is tested is because, based on the characteristic of the localized-based control algorithm, it is expected to be possible to locate any certain point on the vehicle to reduce vertical acceleration. Therefore, this controller will be more effective on extended vehicles such as a limousine as mentioned in Chapter 3.

Figure 40 shows vertical accelerations at the further location.

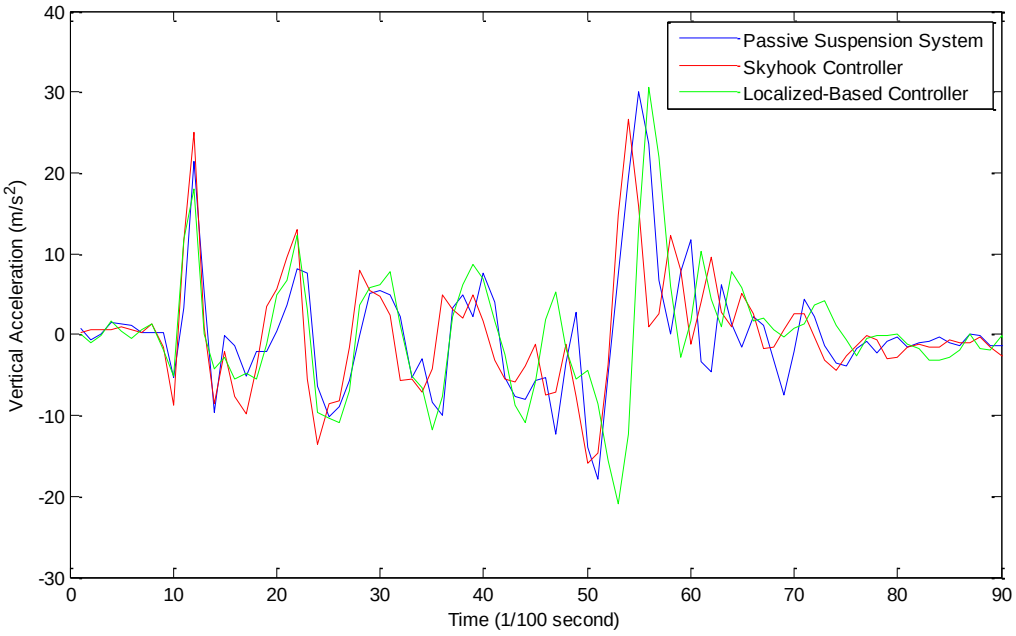

Figure 40: Vertical Acceleration at the Further Location with Different Control Algorithms from the Test Drive

As shown in Figure 40, the maximum peak value of the vertical acceleration is not reduced by using the localized-based controller. The first big peak, however, was reduced by the controller while the skyhook controller does not reduce the first big peak value. However, it reduces the maximum peak of the vertical acceleration. It seems that it would be difficult to compare these control algorithms with only Figure 40.

Table 16: RMS of Vertical Acceleration at the Further Location with Different Control Algorithms from the Test Drive

	RMS	Difference (Relative to Passive)
Passive	7.6354	0 %
Skyhook	7.4121	2.92 %
Localized-Based	7.3941	3.16 %

According to Table 16, it is acknowledged that both controllers play a role to reduce the vertical acceleration at the further location. The relative percentage values of each controller are, however, smaller than those at the rear-left passenger seat location, which is shown earlier. Based on the

simulation shown in Chapter 3, the vertical acceleration at this further location should be impacted by the localized-based controller more than any other locations because of the length between the center of gravity and the further location.

Even though the localized-based Control algorithm is still showing better improvement in terms of RMS values in Table 16, it needs more investigation through examining the case of the further location.

In addition to the vertical acceleration of the vehicle chassis, the motion of the unsprung mass should also be examined. This will indicate the wheel's vertical acceleration – essentially, how road holding of the unsprung mass is on the road.

In this study, Localized-Base controller tuned at the front-left passenger seat location is compared with the passive suspension system and skyhook controller. Since the physical location of the front-left passenger seat is close to the center of gravity of the vehicle, it seems that the localized-based controller does not have effect on the front-left unsprung mass' vertical acceleration, according to Figure 41. Unlike the localized-based controller, the passive suspension system and skyhook controller have similarities of the unsprung mass' vertical acceleration in terms of the peak value and the propensities of the accelerations.

RMS values of the vertical acceleration of each controller are shown in Table 17 below. The skyhook controller shows the best performance to reduce the acceleration of the front-left unsprung mass. The localized-based controller, however, does not improve the performance in terms of RMS value, since it is assumed that the controller only controls the motion of the sprung mass and offers better ride comfort, not road holding. On the other hand, the rear-left unsprung mass seems to be affected by the localized-based controller, as shown in Figure 42. Especially, the maximum peak is reduced by the localized-based controller explicitly.

Table 18 shows the RMS of the rear-left unsprung mass' vertical acceleration of each controller. It indicates that the localized-based controller minimizes the vertical acceleration more than the passive suspension system and skyhook controller. However, the relative difference is small enough to be negligible.

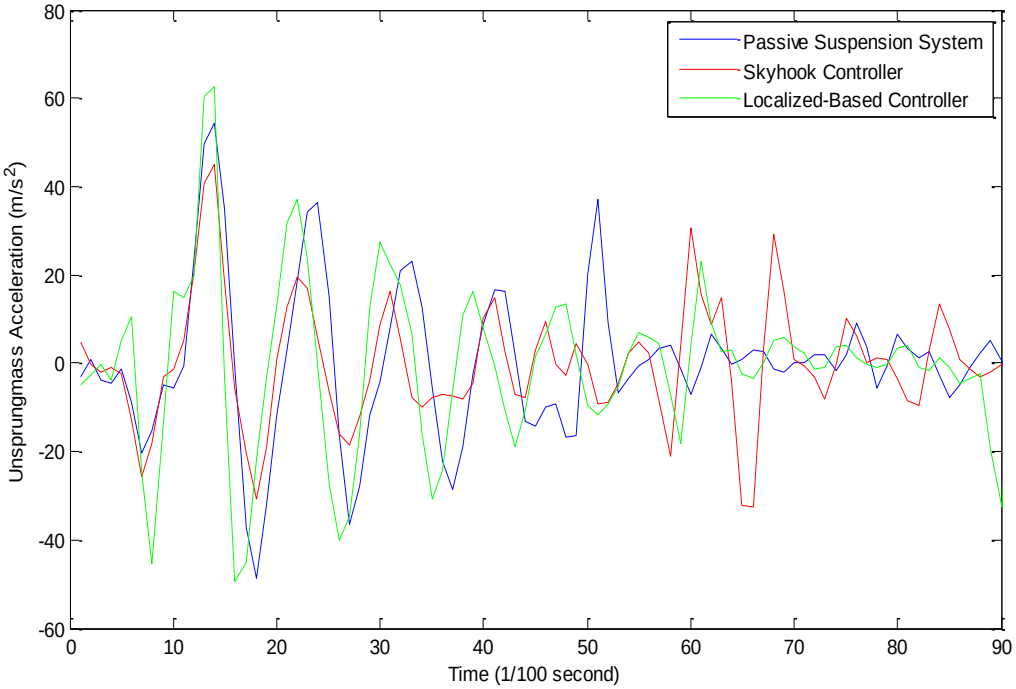

Figure 41: Front Left Unsprung mass' Vertical Acceleration with Localized-Based Controller Tuned at the Front Left Passenger Seat Location

Table 17: RMS of Front Left Unsprung mass' Vertical Acceleration with Localized-Based Controller Tuned at the Front Left Passenger Seat Location

	RMS	Difference (Relative to Passive)
Passive	16.7612	0 %
Skyhook	13.5180	19.35 %
Localized-Based	18.1828	-8.48 %

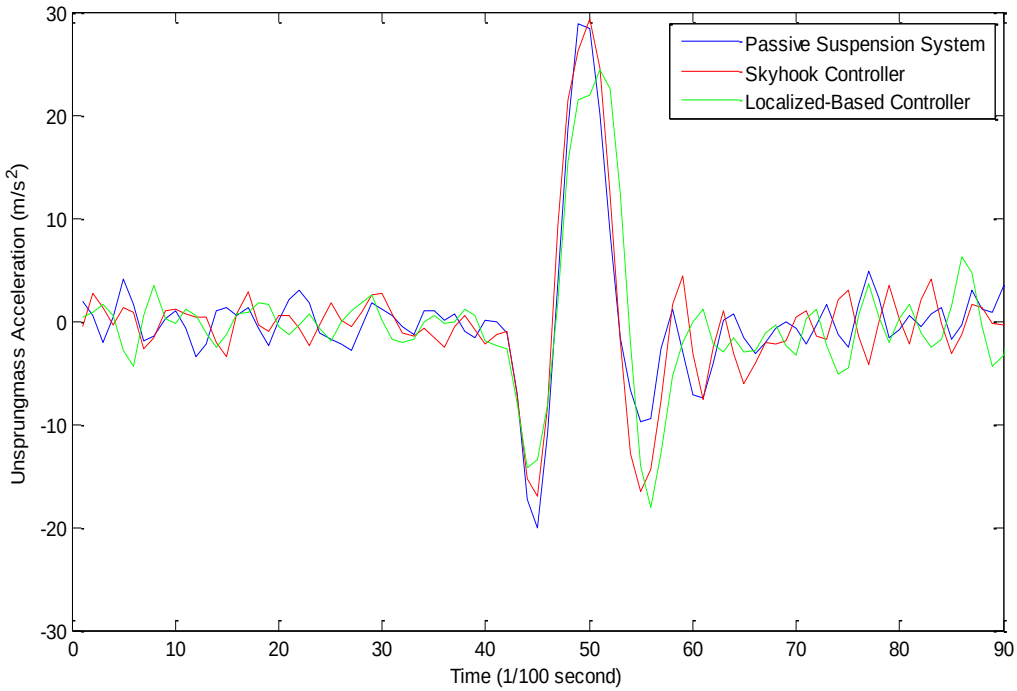

Figure 42: Rear Left Unsprung mass' Vertical Acceleration with Localized-Based Controller Tuned at the Front Left Passenger Seat Location

Table 18: RMS of Rear Left Unsprung mass' Vertical Acceleration with Localized-Based Controller Tuned at the Front Left Passenger Seat Location

	RMS	Difference (Relative to Passive)
Passive	6.5745	0 %
Skyhook	7.0833	-7.74 %
Localized-Based	6.5334	0.63 %

Next, the localized-based controller tuned at the rear-left passenger seat location is compared with the passive suspension system and skyhook controller. Figure 43 shows the front-left unsprung mass' vertical acceleration of each controller. All the vertical acceleration curves of the controllers have similar tendencies before 0.35 seconds. After this time, however, significant peaks randomly happened in all the cases of the controllers. It is assumed that there is some unpredicted noise in the suspension travel sensor while measuring the distance between the sprung mass and the wheel.

Table 19 shows RMS of the front-left unsprung mass' vertical acceleration. As shown, the relative difference between the localized-based controller and passive suspension system is greater than that between the localized-based controller tuned at the front-left passenger seat location and the passive suspension system.

The reasons why this happens are assumed to be as follow:

a) The localized-based controller does not take into account the vertical acceleration of the front-left passenger seat location anymore so that the controller stops reducing the vibration that comes from the front-left unsprung mass to the front-left passenger seat;
b) Different characteristics of the damper on the front and the rear axles;
c) Too much random noise accumulated in the suspension travel sensor

The vibration generated from the front-left unsprung mass can be transmitted to and affect the rear-left passenger seat. However, according to Table 19 and Figure 43, the vibration seems to be dissipated through a structure of the vehicle, and by playing against other vibrations from different passenger seat locations. Even though the tendencies of curves in Figure 44 are seemingly close to each other, Table 20 shows that RMS of the vertical acceleration of the rear-left unsprung mass with the localized-based controller is the worst among the control algorithms.

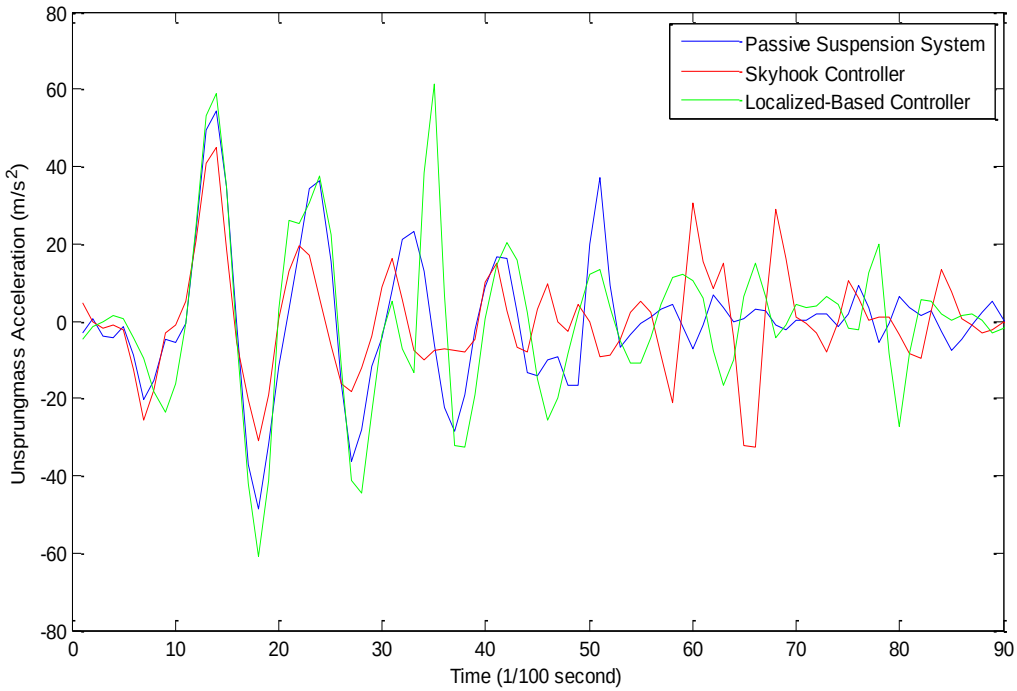

Figure 43: Front Left Unsprung mass' Vertical Acceleration with Localized-Based Controller Tuned at Rear Left Passenger Seat Location

Table 19: RMS of Front Left Unsprung mass' Vertical Acceleration with Localized-Based Controller Tuned at Rear Left Passenger Seat Location

	RMS	Difference (Relative to Passive)
Passive	16.7612	0 %
Skyhook	13.5180	19.35 %
Localized-Based	20.2747	-20.96 %

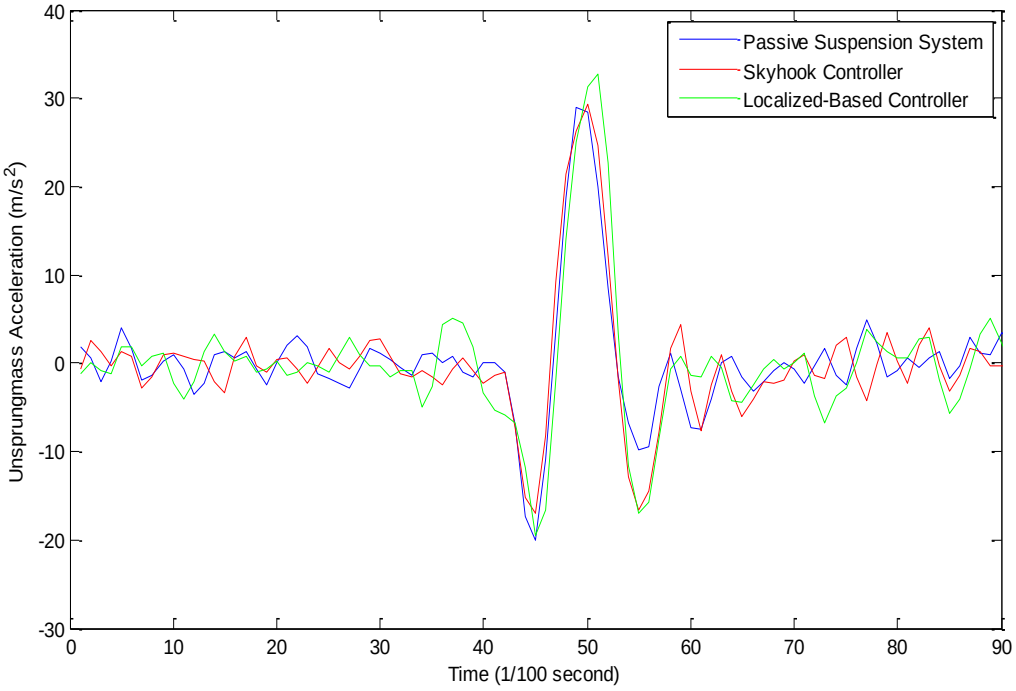

Figure 44: Rear Left Unsprung mass' Vertical Acceleration with Localized-Based Controller Tuned at Rear Left Passenger Seat Location

Table 20: RMS of Rear Left Unsprung mass' Vertical Acceleration with Localized-Based Controller Tuned at Rear Left Passenger Seat Location

	RMS	Difference (Relative to Passive)
Passive	6.5745	0 %
Skyhook	7.0833	-7.74 %
Localized-Based	7.6827	-16.85 %

Lastly, the localized-based controller tuned at the further location is compared with the passive suspension system and skyhook controller. Figure 45 shows the front-left unsprung mass' vertical acceleration. Like the previous front-left unsprung mass' vertical acceleration with the localized-based controller tuned at the rear-left passenger seat location, all three curves seem to have noise that cannot be avoided.

Furthermore, Table 21 indicates the RMS values of each controller. It also shows that the skyhook controller provides better performance regarding the unsprung mass' vertical acceleration in terms of RMS. It can be also assumed that this is because the location of the front-left unsprung mass is relatively close to the center of gravity of the vehicle. The localized-based controller does not exhibit this well, even less than the passive suspension system. It is assumed that, as explained, the localized-based controller does not consider whether the vibration from the front-left wheel affects the front-left passenger seat.

In Figure 46, three controllers show similar tendencies in their curves. However, as shown in Table 22, the skyhook and localized-based controller do not improve the unsprung mass' vertical acceleration.

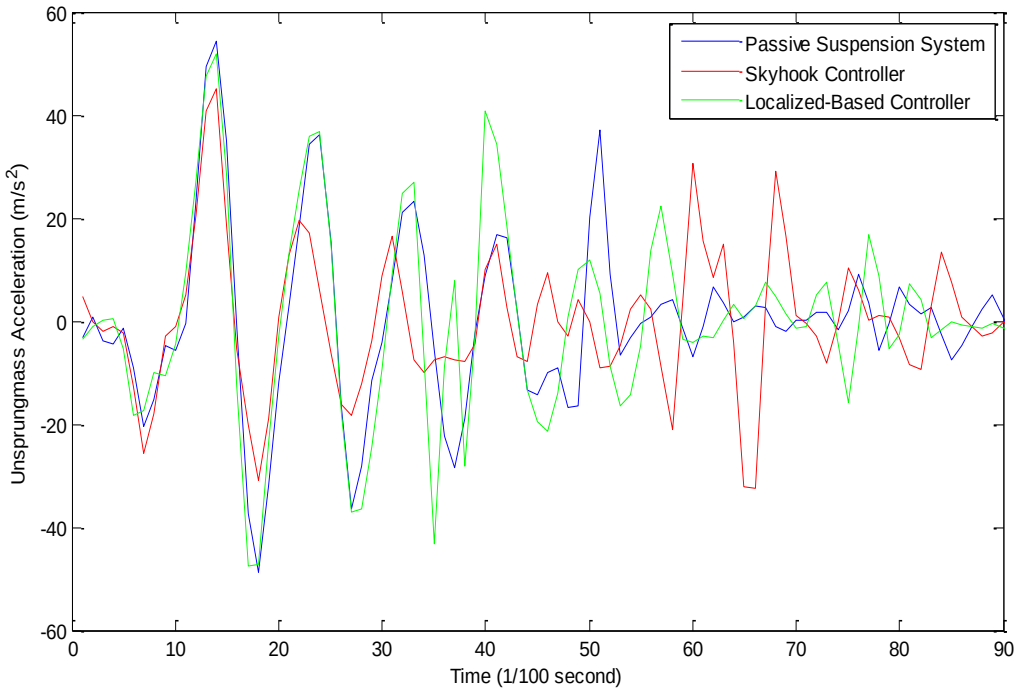

Figure 45: Front Left Unsprung mass' Vertical Acceleration with Localized-Based Controller Tuned at the Further Location

Table 21: RMS of Front Left Unsprung mass' Vertical Acceleration with Localized-Based Controller Tuned at the Further Location

	RMS	Difference (Relative to Passive)
Passive	16.7612	0 %
Skyhook	13.5180	19.35 %
Localized-Based	18.6106	-11.03 %

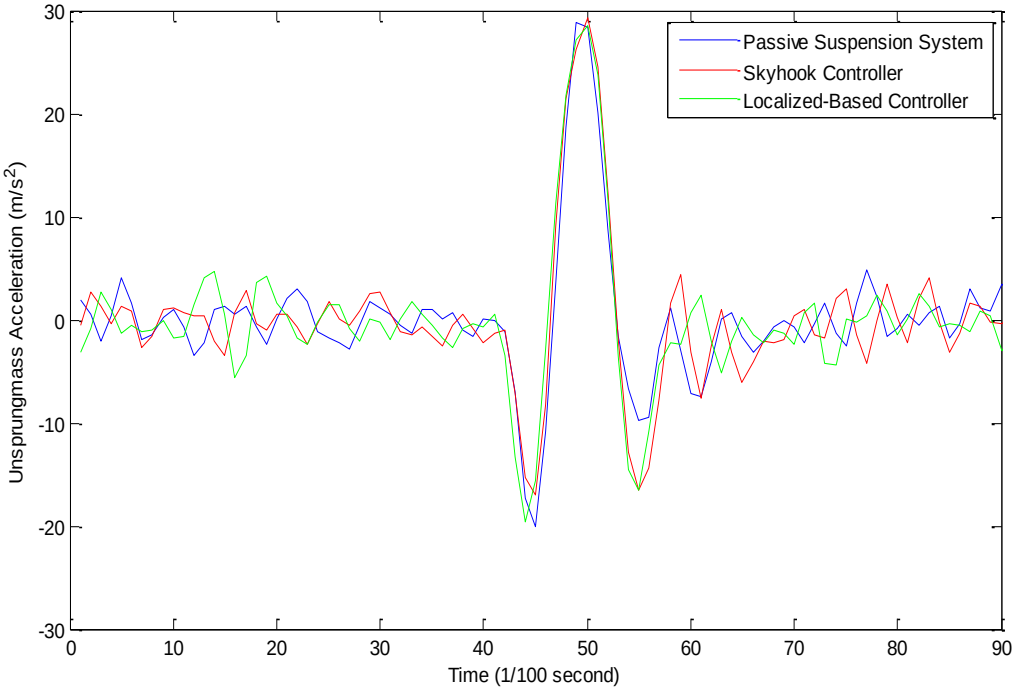

Figure 46: Rear Left Unsprung mass' Vertical Acceleration with Localized-Based Controller Tuned at the Further Location

Table 22: RMS of Rear Left Unsprung mass' Vertical Acceleration with Localized-Based Controller Tuned at the Further Location

	RMS	Difference (Relative to Passive)
Passive	6.5745	0 %
Skyhook	7.0833	-7.74 %
Localized-Based	7.1492	-8.74 %

With the test results, it is shown that the localized-based controller reduced the vertical acceleration of the passenger seat locations, but not the unsprung mass' vertical acceleration. This also explains again that ride comfort conflicts with road holding. Therefore, it is suggested that the localized-based controller should have an independent term in its object function for the vertical acceleration of the unsprung mass.

Chapter 5
Conclusions and Future Work

This thesis introduced a new suspension control system to maximize the ride comfort of any given point in a vehicle.

Using experiments, the performance of the new controller was compared with a passive suspension and a semi-active suspension with a skyhook controller. It was shown that the new control algorithm provides better ride comfort than the passive suspension system and skyhook control algorithm. This was also shown by several simulations in Chapter 3.

To model the damping characteristics of the suspension system of Cadillac STS, the vehicle was driven to have a harsh pitching motion for collecting data. The data was used to develop a model for the MR damper used in the vehicle. The damper was modeled using a linear regression and its inverse model (force to current) was used in the control algorithm. It should be noted that the model of the dampers were obtained directly from the vehicle testing. It would be more appropriate to collect the damper data individually on a test machine to isolate any errors and also expand the speed-force-current results.

The localized-base control algorithm developed in this thesis was mostly for ride comfort. To extend the controller for road holding, a new term for the acceleration of the unsprung mass is needed in the objective function. Further studies are needed for the implementation of the unsprung mass control in the new localized-based algorithm. Another approach could be based on the addition of a separate controller and a weighting function similar to the hybrid controller discussed in Chapter 1.

Bibliography

[1] D. Hrovat, “Applications of optimal control to advanced automotive suspension design,” *J. Dyn. Syst. Meas. Control*, vol. 115, no. 2B, pp. 328–342, 1993.

[2] M. Ahmadian and N. Vahdati, “Transient Dynamics of Semiactive Suspensions with Hybrid Control,” *J. Intell. Mater. Syst. Struct.*, vol. 17, no. 2, pp. 145–153, Feb. 2006.

[3] T. Nath and S. Kumar, “Quarter / Half / Full Car Models for Active Suspension (with PID controller),” in *International Conference on Recent Trends in Engineering and Technology*, 2012, pp. 286–290.

[4] M. Ahmadian and C. A. Pare, “A Quarter-Car Experimental Analysis of Alternative Semiactive Control Methods,” *J. Intell. Mater. Syst. Struct.*, vol. 11, no. 8, pp. 604–612, Aug. 2000.

[5] W. Gao, N. Zhang, and H. P. Du, “A half-car model for dynamic analysis of vehicles with random parameters,” in *Australasian Congress on Applied Mechanics*, 2007, vol. 1, no. December.

[6] J.-S. Lin and C.-J. Huang, “Nonlinear Backstepping Active Suspension Design Applied to a Half-Car Model,” *Veh. Syst. Dyn.*, vol. 42, no. 6, pp. 373–393, Dec. 2004.

[7] A. Stříbrský, K. Hyniová, J. Honců, and A. Kruczek, “Using fuzzy logic to control active suspension system of one-half-car model,” *Acta Montan. Slovaca*, vol. 8, no. 4, pp. 223–227, 2003.

[8] Z. BenLahcene, W. F. Faris, and S. I. Ihsan, “Analysis and simulation of semi-active suspension control policies for two-axle off-road vehicle using full model,” *Int. J. Veh. Syst. Model. Test.*, vol. 6, no. 3/4, pp. 219–231, 2011.

[9] S. Ikenaga, F. L. Lewis, J. Campos, and L. Davis, “Active suspension control of ground vehicle based on a full-vehicle model,” in *American Control Conference*, 2000, no. June, pp. 4019–4024.

[10] B. S. Kim and H. H. Yoo, “Ride comfort uncertainty analysis and reliability design of a passenger vehicle undergoing random road excitation,” *Proc. Inst. Mech. Eng. Part D J. Automob. Eng.*, vol. 227, no. 3, pp. 433–442, Oct. 2013.

[11] C. Longhurst, “Car Bibles. Suspension. http://www.carbibles.com/suspension_bible.html.” [Online]. Available: http://www.carbibles.com/suspension_bible.html.

[12] H. Bolandhemmat, C. M. Clark, and F. Golnaraghi, “Toward systematic approaches to design and implement vehicles semi-active control systems,” in *Industrial Electronics, 2008. ISIE 2008. IEEE International Symposium on*, 2008, no. 1, pp. 817–822.

[13] H. Zhang, E. Wang, F. Min, R. Subash, and C. Su, “Skyhook-based semi-active control of full-vehicle suspension with magneto-rheological dampers,” *Chinese J. Mech. Eng.*, vol. 26, no. 3, pp. 498–505, May 2013.

[14] K. Hudha, H. Jamaluddin, P. M. Samin, and R. A. Rahman, “Effects of control techniques and damper constraint on the performance of a semi-active magnetorheological damper,” *Int. J. Veh. Auton. Syst.*, vol. 3, no. 2/3/4, pp. 230–252, 2005.

[15] E. D. Blanchard, “On the Control Aspects of Semiactive Suspensions for Automobile Applications,” Virginia Tech, 2003.

[16] F. Braghin, F. Resta, and E. Sabbioni, “A modal control for active/semi-active suspension systems,” in *Advanced intelligent mechatronics, 2007 IEEE/ASME international conference on*, 2007, no. Figure 1, pp. 1–6.

[17] M. Biglarbegian, W. Melek, and F. Golnaraghi, “Intelligent Control of Vehicle Semi-Active Suspension Systems for improved Ride Comfort and Road Handling,” in *Fuzzy Information Processing Society, 2006. NAFIPS 2006. Annual meeting of the North American*, 2006, pp. 19–24.

[18] A. Shamsi and N. Choupani, “Continuous and Discontinuous Shock Absorber Control through Skyhook Strategy in Semi-Active Suspension System (4DOF Model),” *World Acad. Sci. Eng. Technol.*, pp. 745–749, 2008.

[19] A. Agrawal, “Performance Improvement of Automotive Suspension Systems using Inerters and an Adaptive Controller,” The University of Waterloo, 2013.

[20] F. J. D. Amato and D. E. Viassolo, “Fuzzy control for active suspensions,” *Mechatronics*, vol. 10, no. 8, pp. 897–920, 2000.

[21] J. Y. Wong, *Theory of Ground Vehicles*. WILEY, 2008.

[22] M. G. Pollard and N. J. A. Simons, “Passenger Comfort—the Role of Active Suspensions,” *Proc. Inst. Mech. Eng. Part D J. Automob. Eng.*, vol. 198, no. 3, pp. 161–175, 1984.

[23] A. Kasaiezadeh, “HCC: Real Time Optimization Algorithm (Introduction).” 2011.

[24] O. Härkegård, “Quadratic Programming Control Allocation Toolbox for Matlab,” 2003. [Online]. Available: http://research.harkegard.se/qcat/.

[25] Oxford Technical Solutions Ltd, “RT2000 Family User Manual,” 2011.

[26] SAE, “Sign Convention for Vehicle Crash Testing,” 1994.

[27] SICK, “DT20-P214B, Short range distance sensors (displacement).” [Online]. Available: https://www.mysick.com/partnerPortal/TopFrameset.aspx?AutoSelect=SK_Products.

[28] DSAPCE, “dSPACE - AutoBox.” [Online]. Available: https://www.dspace.com/en/inc/home/products/hw/accessories/autobox.cfm.

[29] Advanced Motion Controls, “Analog Servo Drive AZ20A8DDC,” 2014.